Combinatorial Polyacrylamide Hydrogels for Preventing Biofouling on Implantable Biosensors

Doreen Chan[1,2,], Jun-Chau Chien[3,*], Eneko Axpe[2], Louis Blankemeier[3], Samuel W. Baker[4], Sarath Swaminathan[5], Victoria A. Piunova[5], Dmitry Yu. Zubarev[5], H. Tom Soh[3,6,7,8,†], Eric A. Appel[2,8,9,10,†]*

[1]Department of Chemistry, Stanford University, Stanford, CA 94305, USA.

[2]Department of Materials Science & Engineering, Stanford University, Stanford, CA 94305, USA.

[3]Department of Electrical Engineering, Stanford University, Stanford, CA 94305, USA.

[4]Department of Comparative Medicine, Stanford University, Stanford, CA 94305, USA.

[5]IBM Almaden Research Center San Jose, CA 95120, USA.

[6]Department of Radiology, Stanford University, Stanford, CA 94305, USA.

[7]Chan Zuckerberg Biohub, San Francisco, CA 94158, USA.

[8]ChEM-H Institute, Stanford University, Stanford, CA 94305, USA.

[9]Department of Bioengineering, Stanford University, Stanford, CA 94305, USA.

[10]Department of Pediatrics (Endocrinology), Stanford University, Stanford, CA 94305, USA.

Keywords: anti-fouling, polymers, biosensors, devices, hydrogels

**These authors contributed equally.*

[†]Correspondance to: eappel@stanford.edu, tsoh@stanford.edu

ABSTRACT

Biofouling on the surface of implanted medical devices severely hinders their functionality and drastically shortens their lifetime. Currently, poly(ethylene glycol) and zwitterionic polymers are considered “gold standards” for device coatings to reduce biofouling. To discover novel anti-biofouling materials, we created a combinatorial library of polyacrylamide-based copolymer hydrogels and screened their ability to prevent fouling from serum and platelet-rich plasma in high-throughput. We found certain non-intuitive copolymer compositions exhibit superior anti-biofouling properties than current gold-standard materials and employed machine learning to identify key molecular features underpinning their performance. For validation, we coated the surfaces of electrochemical biosensors with our hydrogels and evaluated their anti-biofouling performance *in vitro* and in rodent models. Our copolymer hydrogels preserved device function over multiple days and enabled continuous measurements of a small-molecule drug *in vivo*. The novel methodology we describe enables the discovery of anti-biofouling materials that can extend the lifetime of implanted devices.

INTRODUCTION

Medical devices improve the quality of life and extend the lifespan for millions of people worldwide[1]. Yet, when introduced in the body of a patient, biofouling - the non-specific absorption of biomolecules - often occludes these devices and contributes to a reduction in their performance. For devices that contact blood, the adhesion and aggregation of platelets from flowing blood significantly shorten functional device lifetimes[2,3]. Ventricular devices, intravenous cannulas, and stents are all at risk of thrombosis that can increase risk of embolism and stroke[4]. Catheters show signs of biofouling within 24 hours and typically cannot function within 7 days[5]. Once these devices foul, high risk and costly invasive surgeries are often required to replace them, significantly increasing patient and hospital burden. To address these challenges, devices are often coated with a soft material to mitigate biofouling. Approaches to “active” coatings such as drug-eluting[6] or lubricant-infused polymer materials[7] can reduce adhesion and activation of platelets to mitigate biofouling. While these approaches show promise in some applications, they offer only short-term benefits on account of the eventual depletion of the active molecules from the coating material[8-10], leading to major bleeding in patients near the end of the functional device lifetime[11].

On the other hand, passive coating strategies that modify the chemistry at the interface of the devices and bodily fluids are scalable, tunable, and inexpensive. The “gold standard” materials for passive coating strategies are poly(ethylene glycol) (PEG)[12] and its derivatives[13-15], which form a tight hydration layer through hydrogen bonding with water that is hypothesized to contribute to its anti-biofouling properties[16]. Nonetheless, PEG presents several drawbacks including immunogenicity[17,18] and degradation through hydrolysis and auto-oxidation, making it unsuitable for long-term applications with medical devices[19-21]. Many alternatives to PEG have been developed[22], including zwitterionic polymers[23,24], fluoro- and acrylate-based polymers[25-27], and polyglycidols[28]. Yet, these polymers also face issues of degradation and adverse immune responses, or have demonstrated limited translation in preventing non-specific adhesion of

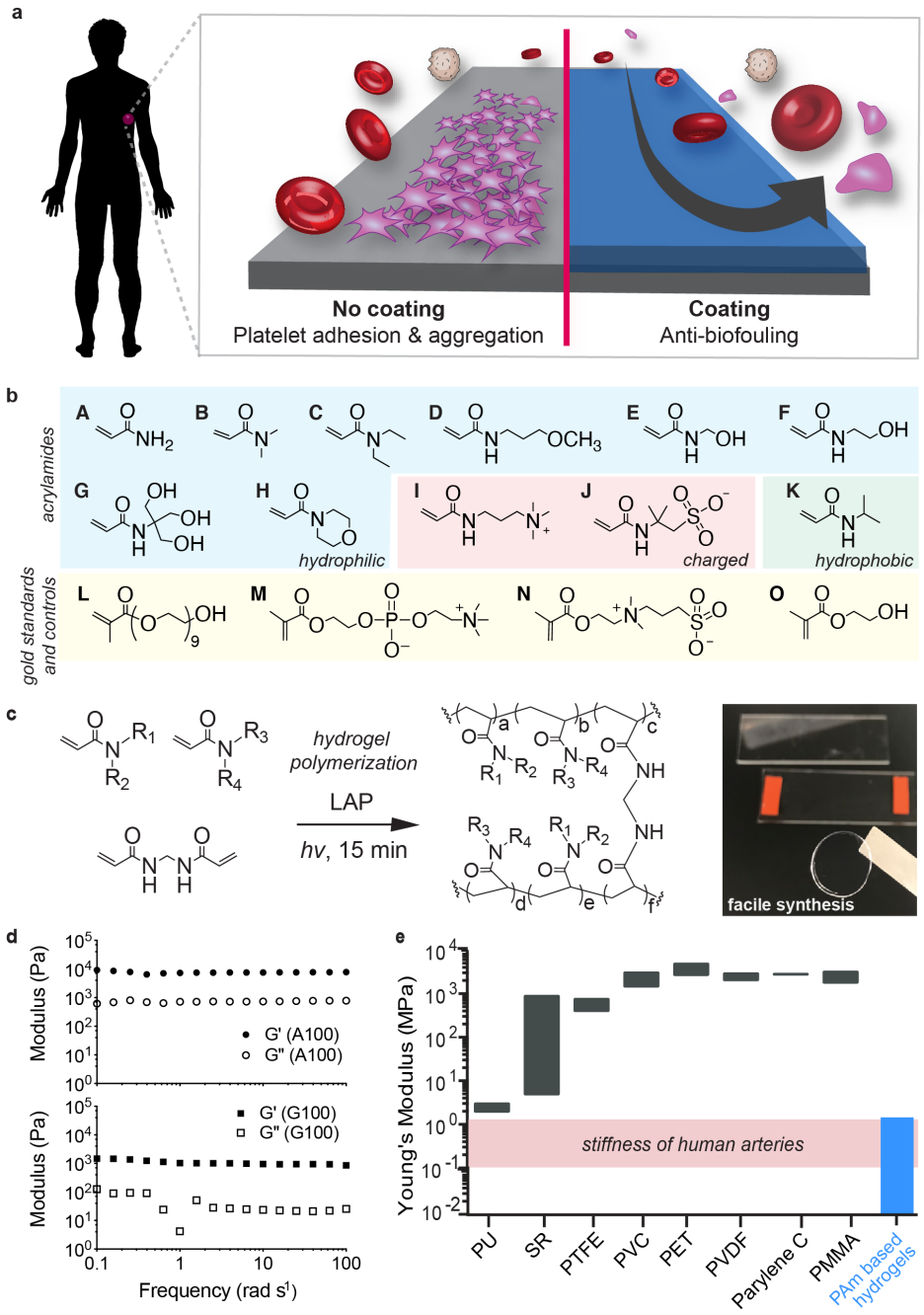

Figure 1. Polyacrylamide hydrogels as anti-biofouling device coatings. a. Coating substrates with anti-biofouling hydrogels can mitigate platelet adhesion and aggregation. **b.** Monomers employed for combinatorial hydrogel synthesis: acrylamide (A), dimethylacrylamide (B), diethylacrylamide (C), (3-methoxypropyl)acrylamide (D), hydroxymethylacrylamide (E), hydroxyethylacrylamide (F), [tris(hydroxymethyl)methyl]acrylamide (G), acryloylmorpholine (H), (acrylamidopropyl)trimethyl-ammonium (I), 2-acrylamido-2-methyl-propane sulfonic acid (J), N-isopropylacrylamide (K), poly(ethylene glycol) methacrylate (L), 2-methacryloyloxyethyl phosphorylcholine (M), [2-(methacryloyloxy)ethyl]dimethyl(3-sulfopropyl)ammonium (N), 2-hydroxyethyl methacrylate (HEMA; O). **c.** Photopolymerization (λ = 350 nm) of polyacrylamide hydrogels using lithium phenyl-2,4,6-trimethylbenzoylphosphinate (LAP) as a radical photointiator. **d.** Oscillatory shear rheology of hydrogels formed with the high (G) and low (A) molecular weight monomers indicates consistency in shear moduli amongst the hydrogels. **e.** Scheme of the range of Young's moduli for commercial polymers: polyurethane (PU), silicone rubbers (SR), polytetrafluoroethylene (PTFE), polyvinyl chloride (PVC), and polyethylene terephthalate (PET), parylene C, and poly(methyl methacrylate) (PMMA). In this study, the polyacrylamide copolymer hydrogels were fabricated with elastic moduli similar to human arteries.

molecules and organisms[29]. There is a critical need for novel approaches to discovery of anti-biofouling materials outperforming conventional polymers such as PEG that make use of performance assays which rigorously test the functionality of these materials.

In this study, we use a high-throughput screening approach to develop new combinatorial copolymer hydrogel materials with remarkable anti-biofouling function, improving upon those of "gold standard" materials and demonstrating both *in vitro* and *in vivo* applicability as coatings on biosensors. We synthesized over 160 copolymer hydrogels through a combinatorial synthesis approach using 11 distinct acrylamide-based monomers and facile photopolymerization techniques (**Fig. 1**). These polyacrylamide hydrogels exhibit tunable mechanical properties and the simplicity of their synthesis makes them highly adaptable for biosensor coatings. Although combinatorial screening approaches have been employed previously for materials discovery efforts[30-32] aimed at mitigating marine or bacterial fouling[33-36], the foreign body response[32,37], or cell adhesion[38,39], to the best of our knowledge, this is the first work to screen for the prevention of platelet adhesion, which is a critical initial process for biofouling in blood. We rigorously assess the anti-fouling behavior of our library of copolymer hydrogels using a high concentration of serum proteins and platelet-rich plasma over prolonged timeframes. Moreover, we used machine learning techniques to elucidate the molecular features of these combinatorial copolymer hydrogels giving rise to their observed biofouling performance. We show that our top-performing copolymer hydrogel is superior to PEG and other conventional anti-biofouling materials for protecting the surfaces of electrochemical biosensors *in vitro* and *in vivo* to enhance device performance and lifetime.

Design of Combinatorial Library of Polyacrylamide Hydrogels for Anti-biofouling

Here we first sought to investigate the ability of a library of chemically distinct polyacrylamide copolymer hydrogels to mitigate blood protein and platelet adhesion (**Fig. 1a**). Several acrylamide-derived monomers have been widely utilized in biological settings (*e.g.*, SDS-PAGE

gels) and in biomedical applications (*e.g.,* contact lenses, fillers, drug delivery materials) and have previously demonstrated potential for use as inert materials in the human body[40,41]. We chose 11 commercially available acrylamide-derived monomers and fabricated a library of 171 polyacrylamide hydrogels comprising unique binary combinatorial mixtures (100:0, 75:25, 50:50, 25:75) of these monomers formulated at 20 wt% monomer (**Fig. 1b, 1c**). These hydrogels were prepared by photopolymerization using lithium phenyl-2,4,6-trimethylbenzoylphosphinate (LAP) as a radical photoinitiator and a simple LED (λ = 350 nm) light source. This weight percent of monomer was chosen to generate hydrogels with stiffness values mimicking those of human vein or artery tissues[42,43] (**Fig. 1d, 1e**). The reactivity ratios for copolymerization of each pair of the members of this diverse array of acrylamide-derived monomers lead to statistical incorporation ($r_1r_2 \approx 1$) of the monomers throughout the hydrogel network[44]. During synthesis, five copolymer formulations turned opaque on account of insolubility of the polymer chains in the aqueous media and were thus omitted from further evaluation. This library of hydrogels is, to our knowledge, the largest combinatorial library of a diverse set of polyacrylamide-based hydrogels generated to date[45].

Protein Adsorption and Platelet Resistant Hydrogels

To rapidly evaluate the extent of biofouling on these hydrogels in a parallel fashion, we developed a high-throughput assay to screen platelet adhesion following incubation in protein serum. While the exact mechanism of biofouling has yet to be precisely elucidated, it is widely hypothesized that such fouling is initiated with the non-specific absorption of proteins from biological milieu[46]. This undesirable binding of proteins to the surface of a biomaterial or device leads to the onset of platelet adhesion and aggregation that eventually cause thrombosis[46-49]. While the majority of anti-biofouling assays appearing in the literature have focused on evaluating adsorption of model proteins at low concentrations (*e.g.*, 1 mg/mL bovine serum albumin[36] or 1 mg/mL fibrinogen[50]) onto materials of interest, these studies do not provide a realistic representation of the complex milieu of biomolecules in blood[51]. Other studies have

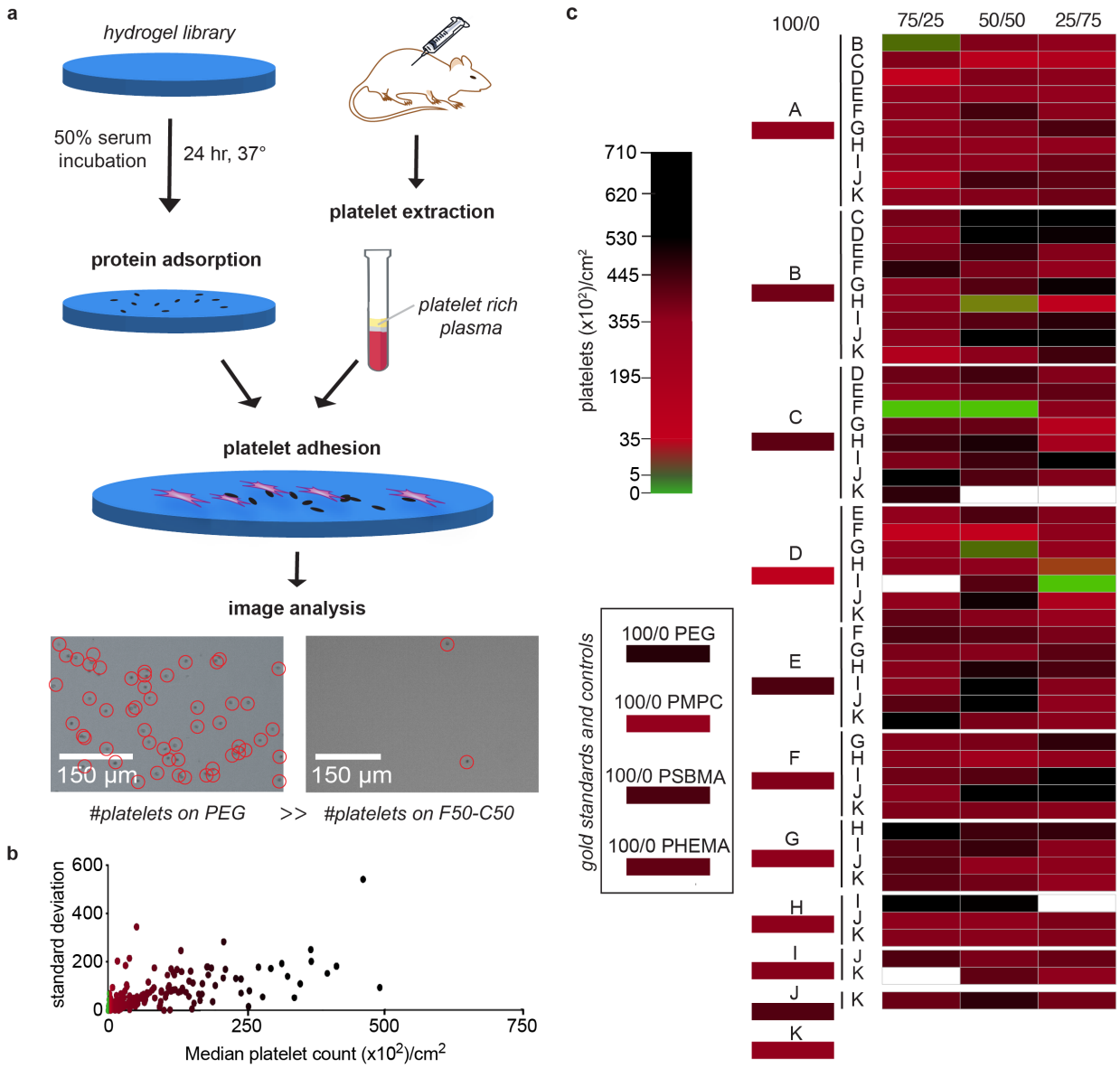

Figure 2. Identification of anti-biofouling acrylamide-based copolymer combinations. a. Hydrogel samples were first incubated in 50% fetal bovine serum for 24 hr at 37°C to ensure extensive protein absorption to the samples. Platelet rich plasma (PRP) obtained from centrifuging rat blood was then incubated on the surface of the hydrogels for 1 hr at 37°C. Several polyacrylamide copolymer hydrogels presented significantly less platelet adhesion than PEG, HEMA, and zwitterionic hydrogel controls. **b.** Standard deviation versus median of the platelet count distribution obtained for each copolymer hydrogel. **c.** Heat map of platelet adhesion counts on copolymer hydrogel samples ordered by the weight ratio of each monomer in the hydrogel formulation (100/0, 25/75, 50/50, 75/25). Colors were assigned to the medians obtained in n ≥ 3 tests.

utilized more relevant mixtures of biological proteins (*e.g.*, fibrinogen, bovine serum albumin, and lysozyme), or diluted or undiluted serum or plasma to evaluate biofouling of new materials, but only over short exposure timeframes ranging from 10-25 minutes[52,23]. The ability to repel whole blood has also been studied; however, in these studies blood was applied to the

biomaterial of interest for only a matter of seconds[53]. Consequently, previous studies have not provided a sufficiently realistic representation of the complex engineering challenge imposed on anti-biofouling coatings in the body on account of low protein concentrations, insufficiently complex biological milieu, and short assay times typically evaluated[51].

To identify anti-biofouling materials from our copolymer hydrogel library with translational potential, therefore, we sought to subject these materials to severe fouling conditions for prolonged periods of time that would nevertheless provide a simple and high-throughput read-out of fouling activity. We chose to use platelet counting to enable a straightforward and realistic metric for anti-biofouling performance of our copolymer hydrogels as platelet adhesion causes occlusion and leads to thrombosis[6]. In these assays, each hydrogel was first incubated in 50% fetal bovine serum (FBS) for 24 hr at 37°C to introduce non-specific protein adsorption (**Fig. 2a**) prior to incubation in platelet-rich plasma for 1 hr at 37°C to introduce platelets that could be counted in an automated fashion. These time points were chosen to allow for distinction between the top formulations while minimizing deviation as greater platelet counts introduced higher variation (**Fig. 2b**). While clear trends in the behaviors of the polyacrylamide copolymers based on their composition were not evident, hydrophobic monomers such as N-isopropylacrylamide (K100) or diethylacrylamide (C100) yielded high platelet counts (20,347 ± 26,609 platelets/cm^2 and 9,583 ± 22 platelets/cm^2, respectively). In contrast, a 50:50 copolymer of hydroxyethylacrylamide (F) and diethylacrylamide (C), denoted F50-C50, yielded the lowest platelet counts (110 ± 20 platelets/cm^2) of all of the materials tested, significantly outperforming PEG (L; 5,000 ± 1,000 platelets/cm^2; $p<0.0001$), 2-methacryloyloxyethyl phosphorylcholine (M; 1,400 ± 450 platelets/cm^2; $p = 0.0008$), HEMA (O; 9,000 ± 1,000 platelets/cm^2; $p<0.0001$), and [(methacryloyloxy)ethyl]-dimethyl(3-sulfopropyl)ammonium zwitterion (N; 13,000 ± 7,000 platelets/cm^2; $p = 0.016$) hydrogel formulations (unpaired *t* test) (**Fig. 2c, Supplementary Fig. S1**). This approach to high-throughput screening of fouling with blood proteins and platelets,

therefore, enabled identification of polyacrylamide-based copolymer hydrogel formulations with superior anti-biofouling properties in comparison to “gold-standard” polymer materials.

Identifying key features of monomers for anti-biofouling properties

To aid in our understanding of the molecular features giving rise to the observed anti-biofouling properties of all of the materials we tested, we analyzed the physicochemical properties of each of the monomers and resulting hydrogels and the contribution of these features to fouling tendencies[54]. The use of platelet counts allowed for inputs that can link polymer behaviors to anti-biofouling performance, in contrast to protein absorption assays that may not yield predictive models[38]. The long-withstanding hypothesis of the anti-fouling mechanism of the “gold-standard” polymers is the presence of a tight hydration layer between the material surface

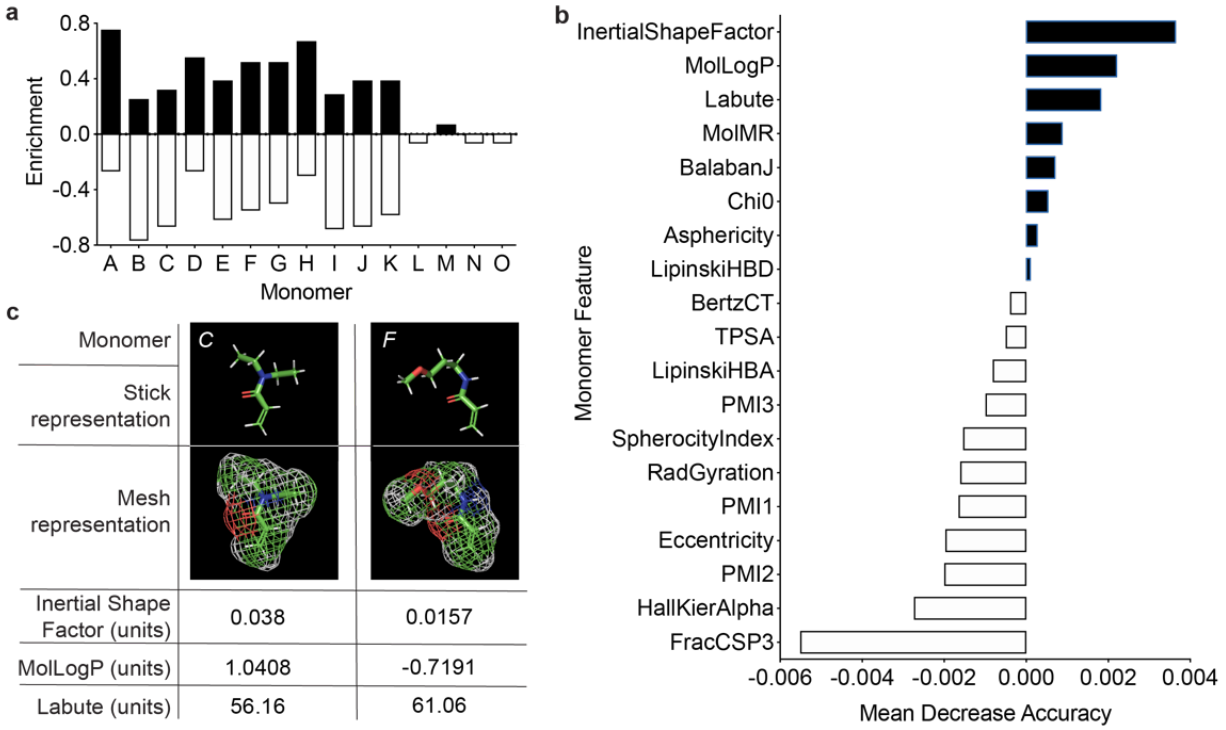

Figure 3. Feature relevance evaluated for monomers using trained random forest models. a. Monomer-specific class enrichment based on raw platelet adhesion data, indicating contribution of individual monomers to anti-biofouling performance. This does not account for the inherent features of the monomers, simply quantification of the contribution of each specific monomer. **b.** MDA of descriptor values evaluated with Feature Set B, summing the importance of the features across all monomers. Positive values (black) indicate that the feature is relevant to model performance, while negative (white) features do not inform the model. **c.** Descriptor values with the highest overall MDA for monomers in the copolymer hydrogel with the best anti-biofouling performance (F50-C50). Descriptors are obtained by transform complex chemical information about the monomer into a number suitable for analysis.

and water that forms a physical and energetic barrier to protein adsorption, determined often by the physicochemical properties of the materials and the surface packing[55]. These properties include surface wettability and hydrophilicity, electrical neutrality, H-bonding, and prevalence of highly hydrated chemical groups. It has also been suggested that surface packing has a role in non-fouling properties, strongly correlated with the ability to form a hydration layer near the surface. Molecular simulations have also suggested that protein adsorption can simply be blocked due to surface density of the polymer at the surface[16]. These prior studies have shown that surface density of grafted polymers resist adherence and that steric repulsion is responsible for preventing protein adsorption as they block the protein adsorption sites[56-58].

Curiously, the composition of the top performing hydrogel formulations yielding the lowest degree of platelet adhesion did not exhibit any intuitive trends, and so we utilized machine learning analysis to identify mechanistic factors underpinning anti-biofouling activity. To analyze the platelet adhesion data, we first classified the copolymer hydrogels as “low platelet count” or “high platelet count” with a random forest model offering robustness to overfitting and the capability to evaluate relevance of data features via mean decrease of accuracy (MDA) (see Methods for technical details). We initially generated a simple feature set (Feature Set A) reflective of the polymer formulation whereby each polymer was represented using one-hot encoding for the alphabet of monomers weighted by the molar ratios of the monomers in the respective copolymer hydrogels. Feature relevance analysis in combination with class-enrichment analysis (**Fig. 3a, Supplementary Fig. S2a**) points to dimethylacrylamide (B), diethylacrylamide (C), and (acrylamidopropyl)trimethylammonium (I) being associated with heavy biofouling. In contrast, acrylamide (A), methoxypropylacrylamide (D), and acryloylmorpholine (H) were prominent monomers in those hydrogel formulations exhibiting excellent anti-biofouling performance. As none of these monomers were in the top anti-biofouling hydrogel formulations, we determined that combinatorial formulations, rather than homopolymer formulations, are crucial in development of robust anti-biofouling coatings.

This consideration motivated two approaches of weighing both the molecular features of each specific monomer and the ratio of each monomer present in a specific formulation. In this feature set, we increased resolution of the molecular features by generating vectors of physicochemical descriptors for the monomers, “inserting” these vectors into one-hot monomer encoding, and weighting by the molar ratios of the monomers in the corresponding copolymer hydrogels (Feature Set B). The f1 score (the overall measure of a model’s accuracy) indicated that these feature sets were suitable in data analysis (**Supplementary Table S1**). Descriptors, in general, are numerical values that capture various characteristics of the molecules, both simple and complex. For example, a feature can be the number of proton donors, or the complexity measure of the molecular graph. The set of descriptors computed for each monomer included 19 values split between physicochemical descriptors (LabuteASA, TPSA, MolLogP, MolMR), molecular graph descriptors (BalabanJ, BertzCT, Chi0, HallKierAlpha), hydrogen-bonding descriptors (LipinskiHBA, LipinskiHBD), and 3D shape descriptors (FracCSP3, InertialShapeFactor, PMI1, PMI2, PMI3, RadGyration, SpherocityIndex, Asphericity, Eccentricity), all as implemented in the *rdkit* library[59] (**Supplementary Table S2**).

Inspection of the feature analysis for the monomers weighted by their molar ratios helps to pinpoint relevant characteristics of the individual monomers. These features can then be expressed as descriptors (**Fig. 3b, Supplementary Table S2, Supplementary Fig. S3**). The top 3 features are from the physicochemical descriptor (MolLogP and Labute) and 3D shape family (InertialShapeFactor). Overall, the most relevant features were found to be connectivity and shape descriptors: (i) Inertial Shape Factor describes the mass distribution in the molecule (by 3 principle moments of inertia), (ii) MolLogP is an estimate of the octanol/water partition coefficient and captures the hydrophilicity/hydrophobicity of the molecule (an energetic characteristic), and (iii) the approximate surface area of the molecule based on the Labute definition. The surface area of the molecules plays a role in anti-biofouling performance as all

monomers have a surface area that is accessible to other molecules (*e.g.* the solvent), and higher values of Labute ASA indicate that “more” surface is accessible (**Fig. 3c**).

In a second approach, we produced a simplified version of the descriptor-based feature set by summing up descriptor vectors of the monomers weighted by their molar ratios in corresponding copolymer hydrogels (Feature Set C), and results indicated the importance of the 3D shape descriptor features (**Supplementary Fig. S2b**). Expanded analysis of the heterogeneity of the platelet count distribution also attributes the importance of a steric mode in the observed fouling (**Supplementary Fig. S4**). Overall, it appears that the relevant molecular features predominantly characterize properties relevant to the steric aspect of the surface formation and geometry of packing of the monomers.

Mechanical Properties of the Top Performing Hydrogel

The mismatch in mechanical properties between many implant materials and native tissues can lead to adverse events such as immune rejection fibrotic responses, trauma, and thrombosis[60]. Thus, it is crucial to match the mechanical properties of the biomaterial with surrounding tissue[61-63]. Hydrogels in particular are widely tunable and have mechanical similarity to biological tissue – in particular the human artery and vein – making them relevant for implanted biosensors[64] (**Supplementary Fig. S5a**). While other coating methods may incorporate polymers via either grafting-to or grafting-from approaches, these coatings are often only nanometers thick and have poor mechanical integrity, making them rather poorly suitable to serve as a soft interface between implanted devices and the body.

We assessed the mechanical properties of our top performing hydrogel through rheology (**Supplementary Fig. S5b, S5c**), interferometry-based nanoindentation, which allows examination of the local microenvironment under wet conditions (**Supplementary Fig. S5d, S5e**), and tensile testing (**Supplementary Fig. S5e**). While soft materials commonly used in the

medical industry exhibit Young's moduli values upwards of several orders of magnitude greater than that of human arteries, our F50-C50 hydrogel coating exhibits mechanical properties that within the regime of human arteries[65], reducing the risk for chronic inflammation and potential failure of the implant[66].

Hydrogel coating of electrochemical biosensors extends sensor lifetime

In order to assess the usefulness of our new copolymer hydrogel material, we tested its anti-biofouling performance in protecting electrochemical biosensors in blood. These biosensors offer a promising strategy for continuously detecting analytes *in vivo*, but their lifetimes are limited by biofouling[55,67]. The degree of biofouling can be quantified using cyclic voltammetry (CV) by measuring the anodic peak current. Through application of a range of voltages through an electrode, electron transfer may be monitored and current intensity monitored through anionic peak. The changes in this peak can be used to assess signal interaction between the electrode surface and $(FeCN_6)^{4-}$ ions in solution and the lifetime and quality of the signal. A larger reduction in signal indicates barriers to the electron transfer process and blocking of ions from diffusing toward the electrode surface due to biofouling[68].

We prepared devices comprising a gold (Au) working electrode (WE), a silver/silver chloride (Ag/AgCl) reference electrode (RE), and a platinum (Pt) counter electrode (CE) (**Fig. 4a, 4b**) with PEG and F50-C50 hydrogel coatings to assess the ability of the hydrogel coating to extend device lifetime. Unprotected (bare) devices were also evaluated as controls. We first performed CV measurements in Na_2EDTA-treated human whole blood spiked with 15 mM of ferrocyanide ions, $(FeCN_6)^{4-}$, to establish a baseline (**Fig. 4c**). Then, devices were incubated in ferrocyanide-free human whole blood mixed with 50 mM of $CaCl_2$ to initiate expedited blood coagulation[69,70] and to directly activate blood platelets (**Fig. S6**). After 2 hr, probes were placed in the same ferrocyanide-spiked blood sample to record CV measurements (**Fig. 4d, 4e, 4f, Supplementary Fig. S7**). A comparable peak reduction was observed for the PEG-coated (50.8 ± 16%) and

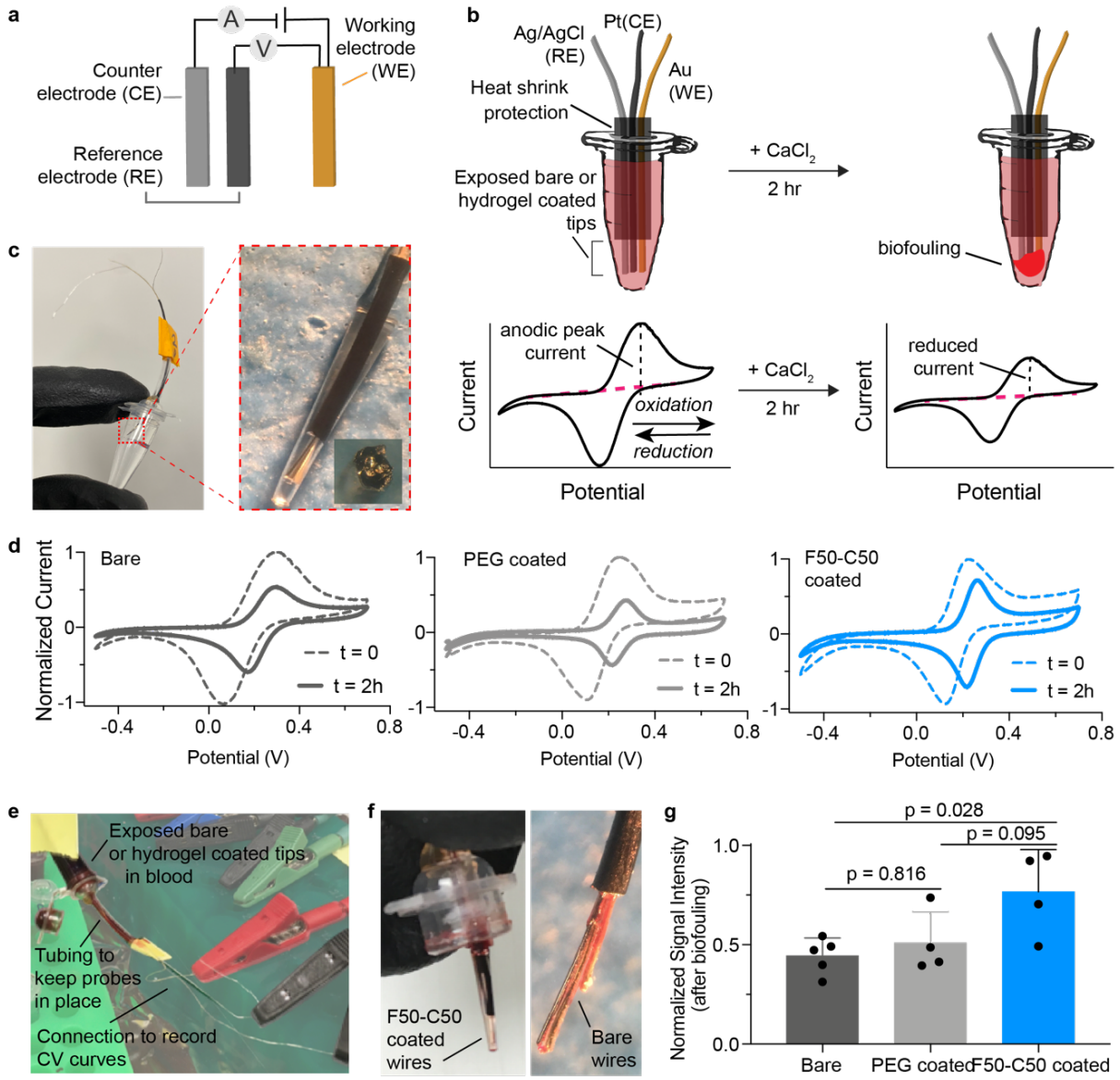

Figure 4. Hydrogel protection of electrochemical device extends lifetime and signal quality over bare and PEG-coated devices. a. Affinity-based electrochemical sensors can be used to detect oxidation of ferrocyanide species $(FeCN_6)^{4-}$. **b.** *in vitro* assay to observe blood fouling on device surface. Probes are inserted through Eppendorf tube to prevent contact with side walls. Biofouling on the device reduces cyclic voltammetry oxidation and reduction peaks. **c.** Probes were coated with a visible layer hydrogel to mitigate biofouling. **d.** CV curves were obtained by cycling electrode between oxidation and reduction potentials of ferrocyanide. Representative graphs are shown before and after $CaCl_2$ addition. **e.** *In vitro* assay setup. Tubes were inverted to ensure probes are completely immersed in blood. **f.** Devices after 2 hr incubation show visible signs of fouling. **g.** Normalized signal intensity, defined by anodic peak current from CV, of devices after biofouling. Data depict mean ± S.D. Significance was determined through a 1-way ANOVA.

bare electrodes (44.3 ± 9%), whereas the F50-C50 hydrogel coating preserved current intensity (76.6 ± 21%) in these assays (**Fig. 4g**). As biofouling could affect both peak intensity and the shape of the CV curves, we evaluated the difference between the oxidation and reduction

potentials, which is referred to as peak band width. A broadening of the peak band width indicates mechanisms other than free diffusion electron potentials or noise in the signal are contributing to device performance and suggests loss in sensitivity[71,72]. We found that both F50-C50-coated and PEG-coated probes exhibited consistent peak band width for forward and reverse scan peaks, indicating that both materials are more effective than the bare probe in reducing signal noise.

Given that our F50-C50 copolymer hydrogel clearly outperformed PEG *in vitro*, we proceeded to test its performance *in vivo*. We implanted the sensing probe into the femoral vein of a rat for 5 days (**Fig. 5a**). This device bundle comprised two WEs (one bare and one F50-C50 coated) and one RE (**Fig. 5b, 5c**), and exhibited a diameter of ~500 μm after the hydrogel coating. CV was performed in $(FeCN_6)^{4-}$-spiked blood sample *in vitro* to determine the anodic current intensity before and after *in vivo* incubation (a fresh Pt probe was included in the measurements for comparison). After 5 days, the sensor was recovered from the femoral vein (**Fig. 5d, 5e**) and F50-C50 hydrogel visibly remained intact on the electrode surface (**Fig. 5f**). Results indicated that F50-C50-coated probes maintain a significantly higher anodic current than unprotected probes (**Fig. 5g, 5h, 5i, Supplementary Fig. S8**).

Hydrogel coating enables real-time measurement *in vivo* via DNA aptamer biosensors

Next, we used our hydrogel to protect "real-time biosensors" that utilize structure-switching aptamers to continuously measure specific analytes *in vivo*[73-76]. Previously, we and other groups have used such sensors to continuously measure the systemic concentrations of small molecule drugs *in vivo*[77,78] and even control their levels using closed-loop feedback control[79]. Briefly, we engineer the aptamers to undergo reversible structure-switching upon target binding, and we conjugate electroactive reporters (*e.g.*, methylene blue, MB) at the distal end of the aptamer (**Fig. 6a**). Then we continuously measure the electron transfer between the reporter and the electrode using cyclic voltammetry. In this way, we can continuously measure the concentration

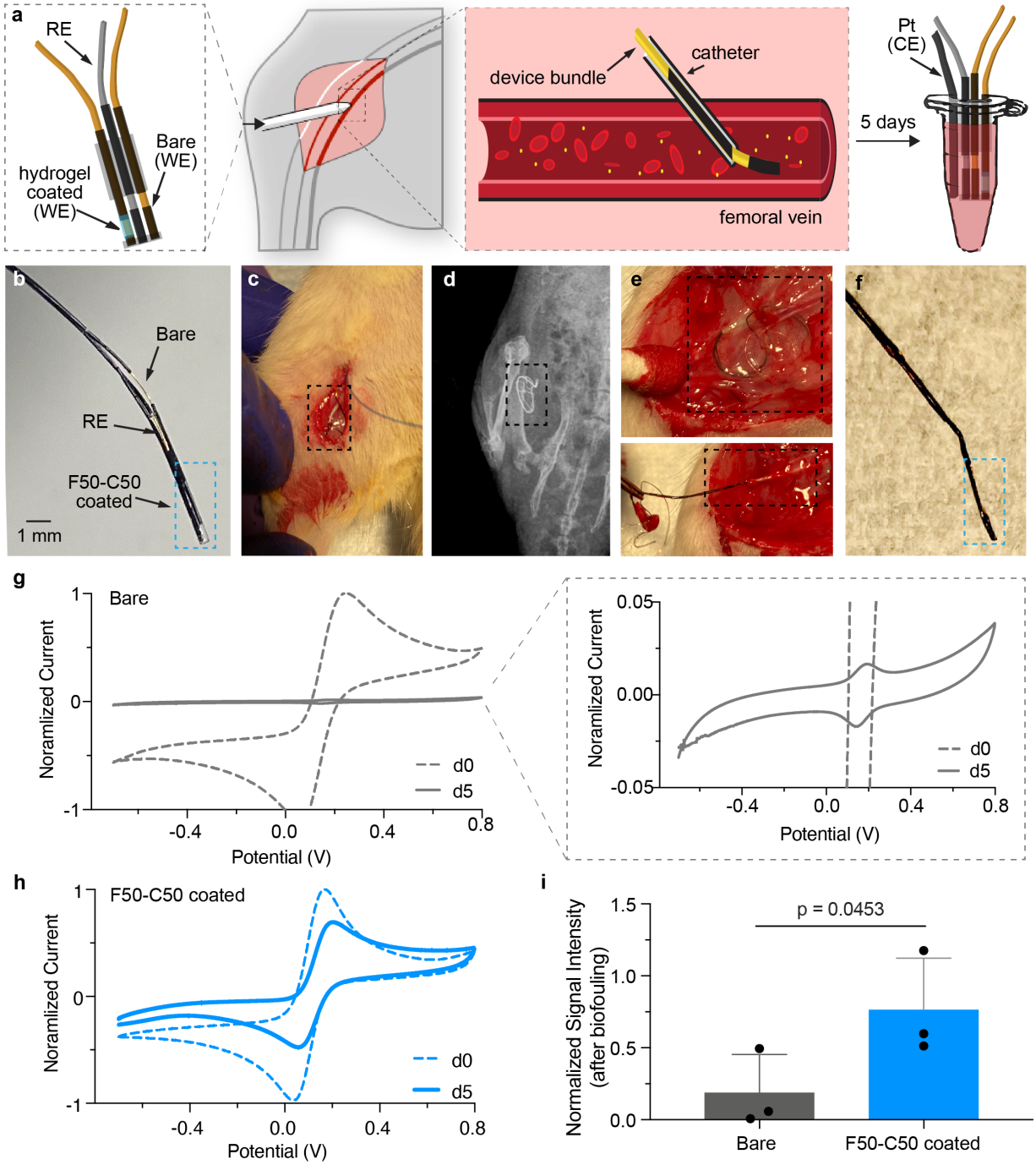

Figure 5. Assessment of F50-C50 hydrogel coating on electrochemical sensor devices *in vivo*. a. Electrochemical probes were incubated in the femoral vein of a rat for 5 days prior to explantation and evaluation of device performance by CV. **b.** Image of electrochemical devices whereby the WE was coated with F50-C50 hydrogels. **c.** Probe insertion into the femoral vein of a rat. **d.** X-ray imaging indicates that the probe remains inserted in the femoral vein after 5 days. **e.** Fibrous encapsulation and removal of electrochemical probes after 5 days *in vivo*. **f.** Image of probe removal indicating the hydrogel coating on the devices remains intact. **g.** Bare probe CV curve after 5 days *in vivo* shows significant signal reduction on account of severe biofouling. **h.** High preservation of CV signal observed for F50-C50-coated probe after 5 days *in vivo*. **i.** Quantification of signal intensity following implantation indicated F50-C50-coated probes exhibit significantly higher signal than bare probes after 5 days (mean ± s.d.; n=3). Data was analyzed with an unpaired one-tailed t-test.

of the analyte in a reagentless manner – in real time. While we and other groups have demonstrated the utility such devices for continuously measuring drug concentrations *in vivo*[80], biofouling of the surfaces of these devices limits their signal quality, and ultimately, their lifetime. Therefore, we sought to investigate the use of our top performing hydrogel coating in improving aptamer-functionalized electrodes performance *in vivo*.

As a model system we employed aminoglycoside aptamers that bind kanamycin, which is a widely used small-molecule antibiotic drug(484.5 Da; diameter ~ 1 nm)[81]. To reduce the diffusion time of the drug to the probe surface, we reduced the thickness of the hydrogel coating by dip-coating the electrodes with precursor solutions for F50-C50 hydrogels and immediately cross-linked by photopolymerization (**Supplementary Fig. S9**). The mesh size of the resulting hydrogel coating was determined to be 2.33 ± 0.07 nm using Fluorescence Recovery After Photobleaching (FRAP), thus allowing free transport of kanamycin. Using such a device, three studies were carried out. Initially, platelet adhesion on probes was characterized following incubation in Na_2EDTA-treated human whole blood for 3 days at room temperature. We observed significantly less platelet adhesion on F50-C50-coated probes when compared with PEG-coated or bare probes (**Supplementary Fig. S10**). Next, aptamer probes were inserted in a circulating blood flowing system for 6 and 12 days (**Supplementary Fig. S11a**). At the end of each assay, the probes were analyzed by SEM, indicating the F50-C50 hydrogel coatings had noticeably less platelet adhesion after both time-points than control probes (**Supplementary Fig. S11b**).

Finally, to test the functional efficacy of these hydrogel coatings *in vivo*, we implanted the aptamer device into the femoral vein of a rat as discussed previously (**Fig. 6b**). Kanamycin (0.1 mL at either 100 or 200 mM) was administered intravenously into the contralateral femoral vein at different time-points. Aptamer activity was measured using square-wave voltammetry (SWV) at 400 and 60 Hz and we used the kinetic differential measurement technique to compensate for

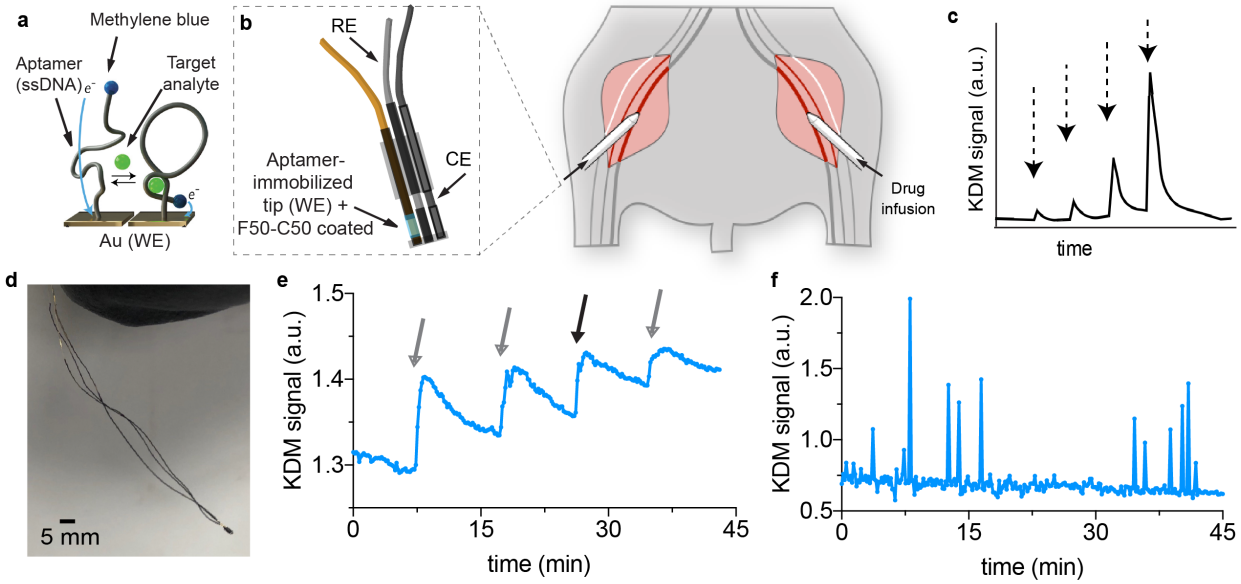

Figure 6. F50-C50 hydrogel coating of a DNA aptamer biosensor enables continuous real-time monitoring of kanamycin *in vivo*. a. DNA aptamers binding with high specificity to a target analyte kanamycin were functionalized on the tip of Au probes. **b.** The probe was inserted into the femoral vein of a rat through a catheter. Kanamycin was infused in the other femoral vein. **c.** The desired kanamycin signal response would exhibit fast kinetics and dose-dependence. **d.** Image of the aptamer probe device**. e.** Real-time *in vivo* sensing of kanamycin after insertion into the rat femoral vein following administration of varying concentrations of the drug by injection into the contralateral vein. Gray arrows represent a 100 µL injection of 100 mM kanamycin and the solid black arrow represents a bolus injection (200 µL) injection of 100 mM kanamycin. **f.** Kanamycin signal for aptamer probe coated with a polyethersulfone membrane *in vivo*. The noise in the data suggests immediate fouling of the membrane.

drift as described previously[77] (**Fig. 6c**, **6d**). After establishing equilibrium over the course of ~95 minutes after implantation, we successfully recorded the real-time drug concentration *in vivo* for the first time with F50-C50-coated devices (**Fig. 6e**). As a control, we prepared a device using a polyethersulfone membrane, a widely used polymer as a filtration membrane[82,83] and protection for biosensor surfaces[84-87] and perform an identical experiment in the rat. As shown in (**Fig. 6f**), we observed extremely noisy signals that do not correlate very well with the kanamycin concentration, clearly indicating that our F50-C50 formulation provides superior protection of the sensor surfaces.

DISCUSSION

In this work we developed a library of 160+ polyacrylamide copolymer hydrogels as anti-biofouling coatings for biomedical devices, the most extensive hydrogel library generated to

date, to identify formulations outperforming current “gold standard” materials such as PEG and zwitterionic polymers. Machine learning analysis of high-throughput fouling analysis suggest relevant mechanisms driving the observed anti-biofouling properties of these materials arise from steric and inertial shape properties of the monomers used in these hydrogels. We demonstrated that the top performing formulation exhibits mechanical properties resembling those of human arteries. Finally, we validated the utility of this hydrogel formulation for improving the performance of biosensor devices both *in vitro* and *in vivo*.

To the best of our knowledge, only a subset of polyacrylamide polymers have been explored as candidates for anti-biofouling coatings, including those derived from acrylamide[52,88], hydroxyethylacrylamide[50,89], (3-methoxypropyl)-acrylamide) and N-isopropylacrylamide[90]. Polyacrylamide-based polymers undergo hydrolysis only under extreme acidic or alkaline (non-biological) conditions and are stable over long time-frames in physiological conditions, thereby enabling their use with medical devices requiring long functional lifetimes[91,92]. While PEG and zwitterionic polymers are considered “gold standard” materials for anti-fouling coatings, our platelet screening assay identified numerous polyacrylamide copolymer hydrogel formulations exhibiting superior anti-biofouling performance, highlighting the promise of polyacrylamide derivatives in these applications. The anti-biofouling behavior of the various copolymer formulations was evaluated using machine learning algorithms with several different feature sets to elucidate the molecular features that give rise to the observed behavior. The features that were common amongst the top performing hydrogel formulations (Feature Set B) were heavy on connectivity and shape descriptors, providing critical insight into the molecular mechanisms underpinning anti-biofouling behaviors and potentially enabling the rational design of next generation coatings. Recently, Rostam *et al.* developed a (meth)acrylate and (meth)acrylamide polymer library to modulate the foreign body response to implanted materials and made use of machine learning approaches to analyze important chemistry descriptors driving macrophage

phenotype and implant fouling. While this study made use of arrays of neat polymers instead of hydrogels, steric (and electronic factors) were also attributed to feature importance[32].

When the top-performing polyacrylamide copolymer hydrogel was used as a coating on an electrochemical biosensor device, little reduction in signal was observed *in vitro* in the presence of whole blood. The mechanism behind this improved signal could be attributed to two critical factors that are enhanced upon application of the hydrogel: (i) size selection of molecular able to reach the probe, and (ii) preclusion of fouling of the probe. First, the surface of a bare electrode is exposed to a broad spectrum of molecules, leading to broad peaks, while the pores of the hydrogel coating exclude molecules too large to diffuse through the matrix, reducing peak widths observed with hydrogel coated probes. Second, the intensity of measured peaks is maintained throughout the duration of the assay with F50-C50 hydrogel-coated probes, suggesting that this formulation precludes biofouling[55,93] while allowing molecules of interest to diffuse through the hydrogel matrix and bind reversibly to the surface to produce signal. In contrast, PEG-coated probes, despite having a comparable mesh size to the F50-C50 hydrogel coating, do not allow for free diffusion of molecules through the coating. Indeed, other studies have suggested PEG coatings may not even be suitable for use on such biosensors as they can hinder electron transfer[94]. Through *in vivo* implantation studies, we showed that the signal reported from bare probes degraded significantly (81 ± 27% reduction) over the 5 day duration of the study, whereas we could obtain clear signals from probes coated with our F50-C50 hydrogel with notably less degradation (24 ± 36% reduction). From these studies, we show that combinatorial screening of copolymer hydrogels offers an exciting avenue for the discovery of anti-biofouling coatings. Although it may not be intuitively obvious from a materials design point-of view, we demonstrate that certain combinations of copolymers can deliver significantly higher anti-biofouling performance in comparison to “gold standard” materials that are typically homopolymers. With further improvements, we believe this strategy of using combinations of acrylamide-based monomers may enable the discovery of anti-biofouling materials offering

long-term implantation of biosensor devices to continuously monitor chronic biomedical conditions.

METHODS

All materials were purchased from Sigma-Aldrich and used as received, unless later specified.

Hydrogel Preparation

Pre-polymer formulations containing 20wt% acrylamide monomer, 1wt% lithium phenyl-2,4,6-trimethylbenzoylphosphinate (LAP) as photo-initiator, and 1wt% methoxy-bisacrylamide were mixed and pipetted between two glass slides separated by a silicone spacer (0.25 mm ± 0.05 mm). Gels were cross-linked in a Luzchem photoreactor system with 8 W bulbs and an intensity of 25-40 W/m^2 (LZC-4, *hv* = 365 nm, 15 min). Due to swelling of polyacrylamides in water, they were placed in 1x PBS for at least 24h before being punched with a 6 mm biopsy punch.

Hydrogel Synthesis Modifications

All AMPSAm formulations were made with slightly basic solution of 2:3 1 M NaOH:water. tHMAm formulations were made with 50:50 DMF:water as well as 100% NiPAm, 75 DEAm, 25 NiPAm and 25 HMAm, 75 NiPAm. PSBMA, PMPC, and MAPAm-based formulations were used with 2x-3x MBAm concentration to achieve comparable mechanical properties. HEMA gels were placed in 50:50 PBS:DMF for 1 hr, 70:30 PBS:DMF for 1 hr and then 100 PBS for 1 day, and comprised 60 mg HEMA and 70 mg PEGdma. PEG gels were 15wt% PEG diacrylate M_n 780 as crosslinker, 5wt% PEG methacrylate M_n 480.

Platelet Adhesion Test

Fresh rat whole blood was mixed in a 10:1 volume ratio of an acid citrate dextrose (ACD) anticoagulant buffer (containing 2.13% free citrate ion, BD Vacutainer Specialty Venous Blood Collection Tubes) for the preparation of platelet-rich plasma (PRP). PRP was obtained via

centrifugation at 600 g for 10 min at 10°C. The platelets were counted using Countess II Automated Cell Counter (ThermoFisher Scientific, USA) and diluted to 2.5 x 10^6 platelets/mL in 1x PBS. 6 mm punches of hydrogels were placed in ultra-low adhesion 96 well plates and incubated for 24 hr at 37°C. Gels were UV sterilized for 5 min prior to incubation with platelets. 100 µL of PRP was pipetted on top of the hydrogels. Platelets were placed on a rotary shaker for 1 hr at room temperature. Platelets were rinsed once with 1x PBS and fixed with 4% PFA. Cells were imaged with EVOS XL Core Imaging System microscope (Life Technologies).

Platelet Detection in Images

Platelets in the images are small round objects approximately 3-4 µm in diameter. Platelet images are of different color and can include various noise, such as gel chunks or dust. The noise typically takes shape of size considerably smaller or larger than platelets. The platelets in the images were detected using difference-of-gaussian approach to the detection. Difference of gaussian was used by blurring images using gaussian kernels of a range of standard deviation in increasing order. Stacks of the differential images between two successively blurred images form a cube and where blobs are local maxima of intensity. Blobs of noisy objects are avoided by tuning the range of standard deviation used in the process.

Fluorescence Recovery After Photobleaching (FRAP)

Hydrogel samples were loaded with 0.5wt% FITC-dextran (4kDa). An Inverted Zeiss LSM 780 Laser Scanning Confocal Microscope (Germany) using a Plan-Apochromat 20X/0.8 M27 objective lens was used for FRAP analysis. We used pixel dwell time 1.58 µs. Samples were photobleached with 405 and 488 argon lasers. All lasers were set at 100% intensity for the bleaching. The samples were placed in a sterile 0.16-0.19 mm thick glass bottom µ-dish from MatTek Corporation (MA, USA). The software used for all FRAP tests was the ZEN lite (Zeiss). To avoid any extra noise, the high voltage was limited to be 700 V. Different tests (n = 5) were made at different locations of the sample. For each test, 10 control pre-bleach images per

second were captured, and bleached the spot with a pixel dwell time of 177.32 μs. 390 post-bleach frames were recorded per second to form the recovery exponential curve. The pixel size was set to be 0.83 μm. The diffusion coefficient was calculated as[95]: D= $\gamma_D(\omega^2/4\tau_{1/2})$ where γ_D = 0.88 for circular beams, ω is the radius of the bleached ROI (12.5 μm), and $\tau_{1/2}$ is the half-time of the recovery. To estimate the mesh size (ξ) of our hydrogels, we used the obstruction theory of Amsden *et al.*:

$$\frac{D}{D_0} = exp\left(-\pi\left(\frac{r_s + r_f}{\xi + 2r_f}\right)^2\right) \quad (1)$$

where D is diffusivity of the solute in the hydrogel, D_0 is the diffusivity of the solute within the liquid in the hydrogel (saline-sodium citrate buffer), assumed to be the same as in pure water, r_s is the radius of the solute (3.51 nm for FITC-dextran 4kDa), r_f is the radius of the polymer chains of the hydrogel the polymer mesh within the hydrogel (estimated to 0.65 nm[96] for the polyacrylamides and 0.51 nm for the PEG[97]) and ξ is the mesh size. The diffusivity (D_0) of a solute in a pure liquid was determined by the hydrodynamic theory, as defined by the Stokes-Einstein equation, to be 69.91 $\mu m^2/s$ using a solution viscosity of η = 0.89 x10^{-4} Pa s.

Scanning Electron Microscopy

SEM images were acquired with an FEI Magellan 400 XHR Microscope with a Beam Voltage of 1 kV. The sample was lyophilized prior to imaging, pressed onto silver paint and sputter-coated with Au:Pd (60:40) before imaging.

Performance Classification

The relevant performance range of the antifouling polymer is platelet count under 100 units. This requirement naturally sets up data analytic task as classification. From this point,

antifouling candidates are considered as members of one of two performance classes. The positive class includes polymers with median platelet count below or equal to 100, and the negative class includes polymers with median platelet above 100 counts. Out of 167 characterized polymers, there are 76 members in the positive class and 91 members in the negative class. The slight class imbalance is considered irrelevant for the practical purposes. It can be mitigated using standard techniques, such as over- and under-sampling. First, the data was organized into three different feature sets (A, B, C). Feature Set A was reflective of the molar ratios of the monomers in the respective polymer. Feature Set B increased granularity by generating vectors of physical-chemical descriptors to the monomer sand weighting these by the molar ratios of the monomer in the polymers. A simplified version was generated in Feature Set C, by summing up descriptor vectors of the monomers weighted by their molar ratios in corresponding polymers. Performance of these classifiers (**Table S2**) showed highest performance with Feature Sets A and B.

Machine Learning Data Analysis

Classification was performed using ensemble of random trees, i.e., random forest model (RF), as implemented in *scikit*-learn 0.20.2. As a model, random forest offers robustness to overfitting and capability to evaluate relevance of data features. RF model parameters were selected via cross-validated grid-search; optimized parameters included the number of estimators, maximum estimator depth, and maximum number of features used in splitting procedure. 3-fold cross-validation was performed over the training set that included 75% of the available observations. Model produced as the result of the cross-validated grid search was tested on the withheld test set that included 25% of the available observations. To evaluate feature relevance, we selected Mean Decrease Accuracy (MDA) following various studies of the performance of different relevance measures. As the measure of feature importance, MDA captures the drop in the accuracy of the trained model under random permutation of the feature whose relevance being evaluated with the rest of the features. Higher positive values of MDA are indicative of the larger

drop in accuracy in the permutation test and point to the higher impact of the respective feature on the model predictions. MDA values close to zero are indicative of non-existing impact of the feature permutation on the accuracy and help identify irrelevant features. Negative MDA values point at features whose permutation in fact increases model accuracy. Such features do not contribute meaningfully to the model performance. Model performance on the test set was evaluated using standard measures of accuracy in classification task, such as recall, accuracy, and f1-score.

Expanded Analysis of Platelet Homogeneity

Coverage profile for each formulation has been generated in the following manner: (i) partition image of the polymer surface into square bins, (ii) count number of platelets (population) in each bin, (iii) generate population histogram for all images obtained for a given formulation, and (iv) normalize histogram by the total number of population bins obtained for a given formulations.

There are several general types of population histograms that one might expect to encounter (**Supplementary Fig. S4a-d**). We recognize that the difference between homogenous and heterogenous coverage modes is quantitative, not qualitative. In both cases, histograms correspond to the distributions that have tails; it is the thickness of the tails that distinguishes the two cases – in homogenous case the tails fall off faster than in heterogenous case.

Using normalized population histograms as features, we performed anomaly detection analysis using Isolation Forest algorithm. Each histogram received an anomaly score; negative values of the score indicate outliers, and positive values indicate inliers. The notions of inliers and outliers are reflective of the structure of the dataset and do not have absolute meaning. The anomaly scores are visualized by reducing dimensionality of the dataset to 2 dimensions via t-SNE manifold embedding and encoding the anomaly score of the samples as the color (**Supplementary Fig. S4i**).

Outlier analysis identifies histograms corresponding to homogenous coverage as the most normal. The change of anomaly score towards the most abnormal system is associated with the increase of heterogeneity of the coverage (**Supplementary Fig. S4j**). Overall, there are 121 systems that bear signs of increasing heterogeneity of the coverage, suggesting that steric mode of fouling plays significant role.

Rheological Characterization

Oscillatory rheology measurements were performed with a TA Instruments AR-G2 rheometer. Amplitude sweeps were conducted at a frequency of 10 rad/s from 0.1-100%. Frequency sweeps were conducted at 0.1% strain from 0.1-100 rad/s. All tests were performed at 25°C using an 8mm parallel plate geometry.

Tensile Test

Tensile strength measurements were performed with an Instron series 5560A with 100 N load cell. Tensile tests were conducted at 0.2 mm/s at room temperature.

Nanoindentation Test

Young's modulus measurements of the hydrogels were performed using a Piuma nanoindenter (Optics11, Netherlands). A probe from the same manufacturer with a stiffness of 38.8 N/m and a tip radius of 27.0 μm was used. Calibration was conducted as on glass under wet conditions as per the manufacturer's instructions. Each sample was immersed in a sterile saline buffer solution (Opti-free® - Replenish, by Alcon®, TX, USA) before the nanoindentation experiments in order to perform force vs distance measurements were conducted under wet conditions. The indentation depth was fixed to be <1 μm in order to avoid bottom effects. At least 8 force curves were used to determine the local Young's modulus of each sample, using the Optics11 Nanoindenter V2.0.27 software. The results are shown as mean ± standard error of the mean. A

Hertzian contact model parameter was used for the fit of the curves assuming that the Poisson's ratio of the samples is $\upsilon = 0.5$.

Fabrication of Electrochemical Biosensors for *In Vitro* Assessment

The working electrode (WE) is prepared with 75-μm diameter gold wire (PFA coated). Ag/Ag Cl wires were prepared by incubating silver electrodes in bleach solution, rinsed vigorously with water, and dried. Pt wire was bundled with Au electrode, following bundling with Ag/AgCl wire to prevent shorting. The tip of the device was cut with a razor blade to expose bare gold and rebleached. No surface roughening is applied. To prevent wires from touching side of Eppendorf tube walls, they were propped in the middle of the tube: a hole was drilled on 0.3 mL Eppendorf tubing to fit 0.04" Tygon tubing. Tygon tubing at 1", inserted into the drilled hold and applied UV-cured epoxy and exposed to 365 nm for 20 seconds. Wires were then inserted through the Tygon tubing into the tube.

Gold, platinum, and silver wires were purchased from A-M Systems Inc (Sequim, WA). 6-Mercapto-1-hexanol and tris(2-carboxyethyl)phosphine were ordered from Sigma Aldrich (St. Louis, MO). EDTA-treated human whole blood for flowing *in vitro* measurements was purchased from BioIVT (Westbury, NY).

Hydrogel Coatings on Electrochemical Biosensors for *In Vitro* Assays

1 μL of prepolymer solution was pipetted into 100 μL pipette tip. Probe were inserted and polymerized for 5 seconds at 365 nm. The pipette tip was removed, and hydrogel coating was visible by eye. Hydrogel was UV cured for an additional 30 seconds.

***In vitro* Assays with Electrochemical Devices**

Probes (bare, PEG-hydrogel coated, and F50-C50 hydrogel coated) were incubated into EDTA-treated human whole blood at room temperature with 250 μL of 15 mM $(FeCN_6)^{4-}$- to record

baseline CV data. Time for this step is limited to 5 minutes to ensure a steady-state readout while minimizing the biofouling. Probes were rinsed in SSC buffer thoroughly to remove any intrinsic fouling and transferred to a 250 µL of whole blood, followed by the addition of $CaCl_2$ to a final concentration of 50 mM. After 2 hr, probes were transferred to the original tube used for baseline measurement. The device is incubated for an additional 5 minutes to allow the diffusion of $(FeCN_6)^{4-}$ throughout the hydrogel. CV scanning on the Au wire was performed (potential range: -0.7 to 0.8 V, step size: 1 mV, scan rate: 0.1 V/sec).

Fabrication of Electrochemical Biosensors for *In Vivo* Assessment

Bare gold was cut into ~10 cm wires. The tip of gold (~1 mm length) was bundled with black medical heat shrink tubing twice (ID 0.006" ± 0.001, Nordson Medical 103-0325). Another 2 layers of heat shrink were applied ~1-2 mm away from the gold shrink, to allow exposure of ~1-2 mm of the bare gold. Ag/AgCl wires were bundled likewise to prevent shorting. Two gold wires (WE) and one Ag/AgCl wire (RE) were bundled at the tip with clear shrink wrap (ID 0.02" ± 0.001, Nordson Medical 103-0249) and at the middle of the probe to provide mechanical strength to the probe when pushing through the catheter.

Hydrogel Coatings on Electrochemical Biosensors for *In Vivo* Assays

For each device, one gold wire was left bare and one gold wire was coated with hydrogel. Prepolymer solution of hydrogel was pipetted into a short segment of tubing from a 26G catheter with inner diameter of 0.6 mm. The device was pushed through the tubing and aligned with one of the two bare gold wires. UV light was applied for 5 seconds and tubing was gently removed. Hydrogel coating was visible on entirety of one gold probe only and UV applied for 25 more seconds to ensure polymerization. Probes were stored in SSC buffer and placed in 200 µL of EDTA-treated rat blood (BioIVT) with 15 mM $(FeCN_6)^{4-}$ to record baseline data. Probes were incubated for 5 minutes to allow diffusion of $(FeCN_6)^{4-}$. CV scanning on the Au wire was performed (potential range: -0.7 to 0.8 V, step size: 1 mV, scan rate: 0.1 V/sec).

In vivo Assays with Electrochemical Devices

Live animal studies were performed using male Sprague–Dawley rats were performed under Stanford APLAC protocol number 33226. All rats used in this work were purchased from Charles River Laboratories at a weight of 350-475 g. The rats were anesthetized using isoflurane gas inhalation (2.5%) and monitored continuously. After exposing femoral vein, a 24 G catheter was implanted into the vein for sensor probe insertion. The needle of the catheter was removed, and the catheter was clipped, protruding from the catheter. Devices were inserted through the catheter and pushed far into the vein. Catheter was clamped and device was secured in place. Incision was sutured. At the end of the experiments, animals were anesthetized using isoflurane gas and devices were removed for immediate measurement in blood used for baseline sample. Rats were then euthanized by exsanguination while under general anesthesia.

Aptamer Device Fabrication and Functionalization

The aminoglycoside aptamer probes were synthesized by Biosearch Technologies with the following sequence: 5′-HS-(CH2)6-GGGACTTGGTTTAGGTAATGAGTCCC-MB-3′. Probes were thiolated at the 5′ end (with a 6-carbon linker) for self-assembly onto the gold working electrodes (WE) and conjugated with a methylene blue (MB) redox label at the 3′ end (with a 7-carbon linker) for charge transfer measurements. The modified DNAs were purified through dual HPLC by the supplier. Upon receipt, the construct was dissolved to 100 μM using UltraPure water (ThermoFischer Scientific Inc.) and frozen at -20°C in individual aliquots at a volume of 1 μL until use. The working electrode (WE) is prepared with 8 cm pure gold wire (at 75 μm diameter) insulated using heat-shrinkable tubing (Nordson Medical, 103-0325) to define the aptamer immobilization surface. The exposed gold wire has a length of 1 ~ 2 mm with an overall surface area range from 0.25 ~ 0.5 mm^2. No surface roughening is applied. Before immobilizing the aptamer probes, the wire is rinsed with acetone, ethanol, deionized water in a sonicator sequentially, followed by electrochemical cleaning. In the latter, cyclic voltammetry (CV) scanning on the gold wire is performed in 500 and 50 mM sulfuric acid solutions (potential

range: -0.4 to 1.5 V, step size: 1 mV, scan rate: 0.1 V/sec), each with three scans. An aliquot of the DNA construct was thawed and reduced for 40 minutes with the addition of 2 μL 100 mM tris(2- carboxyethyl)phosphine at room temperature in dark. The reduced DNA construct is diluted to 1 μM with de-ionized water, and a freshly cleaned gold electrode was immersed for 1 h at room temperature in dark. Next, the sensor is rinsed with de-ionized water for 3 min followed by immersion in 6 mM 6-mercapto-1-hexanol in 1x SSC (saline sodium citrate) buffer for 2 hr to passivate the remaining gold surface and remove nonspecifically adsorbed DNA, also at room temperature in dark. The sensor was rinsed with de-ionized water for another 3 min and stored in 1x SSC buffer in 4°C for 12 h before the application of the hydrogel.

Electrochemical measurements were conducted using an electrochemical analyzer (EmStat Blue, Palm Instruments BV) in square-wave-voltammetry (SWV) mode. As only working and reference electrodes are employed in the device, the input connections for the reference and the counter electrode from the electrochemical analyzer are shorted. The working electrode is scanned in continuous succession with a scan period of 2 seconds, alternating between two SWV frequencies (400 and 60 Hz) at a constant SWV amplitude of 36 mV. Two frequencies are used in order to apply kinetic differential measurements for drift mitigation. As the MB redox peak was typically observed at about -350 mV in our setup, a potential range of -500 to -100 mV (with respect to Ag/AgCl reference) is selected during SWV scan. A custom peak-fitting script was created to fit the SWV measurements with a Gaussian curve on a hyperbolic base-line. Peak currents were then normalized to a baseline peak current to generate the signal gain. All reported gains were obtained via KDM with the difference divided by the average of gains from 400 and 60 Hz signals. Kanamycin monosulfate was ordered in USP grade from Gold BioTechnology, Inc (St. Louis, MO).

Hydrogel Coatings on Aptamer Devices

Acrylamide monomers were purified through basic alumina column. The hydrogel is applied to the sensing gold wire through capillary force, in which the sensor is dipped into the unlinked hydrogel solution for 5 sec and removed immediately. The hydrogel is then polymerized by applying 365 nm UV light for 30 sec. No reduction in the MB peak current is observed after UV application. An Ag/AgCl reference electrode (a 75 μm diameter Ag wire chlorinated in bleach overnight) is attached to the hydrogel-coated gold wire using heat shrinkable tubing. The final device is placed in 1x SSC buffer at 4 °C overnight before use.

In vitro Assessments of Aptamer Devices in Stationary and Flowing Blood

Aptamer devices were incubated in EDTA-treated human whole blood (Bio-IVT) or inserted via a catheter to a flowing blood set-up for 6 or 12 days room temperature. Probes were immersed in 2.5% GFA for 15 minutes and rinsed with PBS. Probes were freeze dried, lyophilized and coated with Au:Pd for SEM imaging.

In vivo Assessment of Aptamer Devices

Live animal studies were performed using Sprague–Dawley rats under Stanford APLAC protocol number 33226. Male rats were purchased from Charles River Laboratories at a weight of 300 - 350 g. The rats were anesthetized using isoflurane gas inhalation (2.5%) and monitored continuously. After exposing both femoral veins, a 20G catheter was implanted into the left femoral vein for sensor probe insertion whereas a 22G catheter was implanted into the right femoral vein for drug infusion. 0.1 - 0.3 mL of heparin (1000 U/mL, SAGENT Pharmaceuticals, Schaumburg, IL, USA) were immediately infused through the catheter to prevent blood clotting. The sensor was secured in place with surgical suture after the insertion. A sequence of bolus injection is performed manually using a 5 mL syringe. In each injection, 100 or 200 μL of 100 mM kanamycin in PBS buffer was injected through the sensor-free catheter. At the end of the experiments, animals were euthanized by exsanguination while under general anesthesia.

Statistical Analysis

All values of significance were determined using a one-way ANOVA or student's t-test with Prism GraphPad 8.4 software.

Ethical Statement

All animal procedures were performed according to Stanford APLAC approved protocols.

Acknowledgements

Doreen Chan is grateful for an award by the Department of Defense, Air Force Office of Scientific Research, National Defense Science and Engineering Graduate (ND-SEG) Fellowship, 32 CFR 168a with government support under FA9550-11-C-0028. Dr. Eneko Axpe is thankful for funding support from a Stanford Bio-X Interdisciplinary Initiative Program Round 8 (2016) Seed Grant and the European Commission for the Marie Curie global fellowship. Part of this work was performed at the Stanford Nano Shared Facilities (SNSF), supported by the National Science Foundation under award ECCS-1542152.

Author contributions

D.C., J.-C.C., E.A., S.S., V.A.P., D.Yu.Z., H.T.S., and E.A.A. designed experiments. D.C., J.-C.C., E.A., L.B., S.S., V.A.P., D.Yu.Z., H.T.S., and E.A.A. conducted experiments. S.W.B. assisted with surgeries. D.C., J.-C.C., E.A., L.B., H.T.S., and E.A.A. analyzed data. D.C., E.A., S.S., V.A.P., D.Yu.Z., H.T.S., and E.A.A. wrote the paper.

Competing Interests

D.C., J.-C.C., E.A., H.T.S., and E.A.A are listed as authors on a provisional patent application describing the technology reported in this manuscript.

REFERENCES

1. Harding, J. L. & Reynolds, M. M. Combating medical device fouling. *Trends Biotechnol* **32**, 140-146, (2014).

2. Pitt, W. G., Park, K. & Cooper, S. L. Sequential Protein Adsorption and Thrombus Deposition on Polymeric Biomaterials. *Journal of Colloid and Interface Science* **111**, 343-362, (1985).

3. Zhang, T., Zhang, X. & Deng, X. Applications of protein resistant polymer and hydrogel coatings on biosensors and biomaterials. *Annals of Biotechnology* **2**, 1-7, (2018).

4. Jaffer, I. H. & Weitz, J. I. The blood compatibility challenge. Part 1: Blood-contacting medical devices: The scope of the problem. *Acta Biomater* **94**, 2-10, (2019).

5. Singha, P., Locklin, J. & Handa, H. A review of the recent advances in antimicrobial coatings for urinary catheters. *Acta Biomater* **50**, 20-40, (2017).

6. Goudie, M. J., Pant, J. & Handa, H. Liquid-infused nitric oxide-releasing (LINORel) silicone for decreased fouling, thrombosis, and infection of medical devices. *Sci Rep* **7**, 13623, (2017).

7. Epstein, A. K., Wong, T. S., Belisle, R. A., Boggs, E. M. & Aizenberg, J. Liquid-infused structured surfaces with exceptional anti-biofouling performance. *Proc Natl Acad Sci U S A* **109**, 13182-13187, (2012).

8. Leslie, D. C. *et al.* A bioinspired omniphobic surface coating on medical devices prevents thrombosis and biofouling. *Nat Biotechnol* **32**, 1134-1140, (2014).

9. MacCallum, N. *et al.* Liquid-Infused Silicone As a Biofouling-Free Medical Material. *ACS Biomaterials Science & Engineering* **1**, 43-51, (2014).

10. Amini, S. *et al.* Preventing mussel adhesion using lubricant-infused materials. *Science* **357**, 668-673, (2017).

11. Keefer, L. K. Thwarting thrombus. *Nature Materials* **2**, 357-358, (2003).

12. Zhang, M., Desai, T. & Ferrari, M. Proteins and cells on PEG immobilized silicon surfaces. *Biomaterials* **19**, 953-960, (1998).

13. Jo, S. & Park, K. Surface modification using silanated poly(ethylene glycol)s. *Biomaterials* **21**, 605-616, (2000).

14. Hawkins, M. L. & Grunlan, M. A. The protein resistance of silicones prepared with a PEO-silane amphiphile. *Journal of Materials Chemistry* **22**, (2012).

15. Hawkins, M. L. *et al.* Anti-protein and anti-bacterial behavior of amphiphilic silicones. *Polym Chem* **8**, 5239-5251, (2017).

16. Chen, S., Li, L., Zhao, C. & Zheng, J. Surface hydration: Principles and applications toward low-fouling/nonfouling biomaterials. *Polymer* **51**, 5283-5293, (2010).

17. Armstrong, J. K. *et al.* Antibody against poly(ethylene glycol) adversely affects PEG-asparaginase therapy in acute lymphoblastic leukemia patients. *Cancer* **110**, 103-111, (2007).

18. Chang, C. J. *et al.* A genome-wide association study identifies a novel susceptibility locus for the immunogenicity of polyethylene glycol. *Nat Commun* **8**, 522, (2017).

19. Herold, D. A., Keil, K. & Bruns, D. E. Oxidation of Polyethylene Glycols by Alcohol Dehydrogenase. *Biochemical Pharmacology* **38**, 73-76, (1989).

20. Ostuni, E. *et al.* Self-Assembled Monolayers That Resist the Adsorption of Proteins and the Adhesion of Bacterial and Mammalian Cells. *Langmuir* **17**, 6336-6343, (2001).

21. Zustiak, S. P. & Leach, J. B. Hydrolytically degradable poly(ethylene glycol) hydrogel scaffolds with tunable degradation and mechanical properties. *Biomacromolecules* **11**, 1348-1357, (2010).

22. Ngo, B. K. D. & Grunlan, M. A. Protein Resistant Polymeric Biomaterials. *ACS Macro Letters* **6**, 992-1000, (2017).

23. Jiang, S. & Cao, Z. Ultralow-fouling, functionalizable, and hydrolyzable zwitterionic materials and their derivatives for biological applications. *Adv Mater* **22**, 920-932, (2010).

24. Laschewsky, A. Structures and Synthesis of Zwitterionic Polymers. *Polymers* **6**, 1544-1601, (2014).

25. Vercellotti, G. M., Hammerschmidt, D. E., Craddock, P. R. & Jacob, H. S. Activation of Plasma Complement by Perfluorocarbon Artificial Blood: Probably Mechanism of Adverse Pulmonary Reactions in Treated Patients and Rationale for Corticosteroid Prophylaxis. *Blood* **59**, 1299-1304, (1982).

26. Wang, Z. & Zuilhof, H. Antifouling Properties of Fluoropolymer Brushes toward Organic Polymers: The Influence of Composition, Thickness, Brush Architecture, and Annealing. *Langmuir* **32**, 6571-6581, (2016).

27. Chen, P. R., Wang, T. C., Chen, S. T., Chen, H. Y. & Tsai, W. B. Development of Antifouling Hyperbranched Polyglycerol Layers on Hydroxyl Poly-p-xylylene Coatings. *Langmuir* **33**, 14657-14662, (2017).

28. Gam-Derouich, S. *et al.* Highly hydrophilic surfaces from polyglycidol grafts with dual antifouling and specific protein recognition properties. *Langmuir* **27**, 9285-9294, (2011).

29. Chen, S. *et al.* Exploring the Biocompatibility of Zwitterionic Copolymers for Controlling Macrophage Phagocytosis of Bacteria. *Macromol Biosci* **16**, 1714-1722, (2016).

30. Smith, J. R. *et al.* Integration of Combinatorial Synthesis, Rapid Screening, and Computational Modeling in Biomaterials Development. *Macromolecular Rapid Communications* **25**, 127-140, (2004).

31. Webster, D. C., Chisholm, B. J. & Stafslien, S. J. Mini-review: combinatorial approaches for the design of novel coating systems. *Biofouling* **23**, 179-192, (2007).

32. Rostam, H. M. *et al.* Immune-Instructive Polymers Control Macrophage Phenotype and Modulate the Foreign Body Response*In Vivo*. *Matter* **2**, 1-18, (2020).

33. Fletcher, J. T., Finlay, J. A., Callow, M. E., Callow, J. A. & Ghadiri, M. R. A combinatorial approach to the discovery of biocidal six-residue cyclic D,L-alpha-peptides against the bacteria methicillin-resistant Staphylococcus aureus (MRSA) and E. coli and the biofouling algae Ulva linza and Navicula perminuta. *Chemistry* **13**, 4008-4013, (2007).

34. Pieper, R. J. *et al.* Combinatorial approach to study the effect of acrylic polyol composition on the properties of crosslinked siloxane-polyurethane fouling-release coatings. *Journal of Coatings Technology and Research* **4**, 453-461, (2007).

35. Hook, A. L. *et al.* Combinatorial discovery of polymers resistant to bacterial attachment. *Nat Biotechnol* **30**, 868-875, (2012).

36. Gu, M. *et al.* Combinatorial synthesis with high throughput discovery of protein-resistant membrane surfaces. *Biomaterials* **34**, 6133-6138, (2013).

37. Vegas, A. J. *et al.* Combinatorial hydrogel library enables identification of materials that mitigate the foreign body response in primates. *Nat Biotechnol* **34**, 345-352, (2016).

38. Mei, Y. *et al.* Combinatorial development of biomaterials for clonal growth of human pluripotent stem cells. *Nat Mater* **9**, 768-778, (2010).

39. Celiz, A. D. *et al.* Chemically diverse polymer microarrays and high throughput surface characterisation: a method for discovery of materials for stem cell culturedaggerElectronic supplementary information (ESI) available. See DOI: 10.1039/c4bm00054dClick here for additional data file. *Biomater Sci* **2**, 1604-1611, (2014).

40. Xi, T. F. *et al.* Cytotoxicity and altered c-myc gene expression by medical polyacrylamide hydrogel. *J Biomed Mater Res A* **78**, 283-290, (2006).

41. Sun, J. Y. *et al.* Highly stretchable and tough hydrogels. *Nature* **489**, 133-136, (2012).

42. Alhosseini Hamedani, B., Navidbakhsh, M. & Ahmadi Tafti, H. Comparison between mechanical properties of human saphenous vein and umbilical vein. *BioMedical Engineering OnLine* **11**, 1-15, (2012).

43. Khamdaeng, T., Luo, J., Vappou, J., Terdtoon, P. & Konofagou, E. E. Arterial stiffness identification of the human carotid artery using the stress-strain relationship in vivo. *Ultrasonics* **52**, 402-411, (2012).

44. Kuo, J. & Chen, C. A Method of Calculating Copolymerization Reactivity Ratios. *Journal of Applied Polymer Science* **26**, 1117-1128, (1981).

45. De Hoe, G. X. *et al.* Sustainable Polyester Elastomers from Lactones: Synthesis, Properties, and Enzymatic Hydrolyzability. *J Am Chem Soc* **140**, 963-973, (2018).

46. Gifford, R. *et al.* Protein interactions with subcutaneously implanted biosensors. *Biomaterials* **27**, 2587-2598, (2006).

47. Brash, J. L. Hydrophobic Polymer Surfaces and their Interactions with Blood. Vol. 283 356-371 (The New York Academy of Sciences, 1977).

48. Vaddiraju, S., Burgess, D. J., Tomazos, I., Jain, F. C. & Papadimitrakopoulos, F. Technologies for Continuous Glucose Monitoring: Current Problems and Future Promises. *Jounral of Diabetes Science and Technology* **4**, 1540-1562, (2010).

49. Wörz, A., Berchtold, B., Moosmann, K., Prucker, O. & Rühe, J. Protein-resistant polymer surfaces. *Journal of Materials Chemistry* **22**, (2012).

50. Zhao, C. *et al.* Dual functionality of antimicrobial and antifouling of poly(N-hydroxyethylacrylamide)/salicylate hydrogels. *Langmuir* **29**, 1517-1524, (2013).

51. Park, K., Shim, H. S., Dewanjee, M. K. & Eigler, N. L. In vitro and in vivo studies of PEO-grafted blood-contacting cardiovascular prostheses. *Journal of Biomaterials Science, Polymer Edition* **11**, 1121-1134, (2012).

52. Liu, Q., Singh, A., Lalani, R. & Liu, L. Ultralow fouling polyacrylamide on gold surfaces via surface-initiated atom transfer radical polymerization. *Biomacromolecules* **13**, 1086-1092, (2012).

53. Wong, T. S. *et al.* Bioinspired self-repairing slippery surfaces with pressure-stable omniphobicity. *Nature* **477**, 443-447, (2011).

54. Le, T. C., Penna, M., Winkler, D. A. & Yarovsky, I. Quantitative design rules for protein-resistant surface coatings using machine learning. *Sci Rep* **9**, 265, (2019).

55. Liu, N., Xu, Z., Morrin, A. & Luo, X. Low fouling strategies for electrochemical biosensors targeting disease biomarkers. *Analytical Methods* **11**, 702-711, (2019).

56. Jeon, S. I., Lee, J. H., Andrade, J. D. & De Gennes, P. G. Protein-Surface Interactions in the Presence of Polyethylene Oxide. *Journal of Colloid and Interface Science* **142**, 149-158, (1991).

57. Szleifer, I. Protein Adsorption on Surfaces with Grafted Polymers: A Theoretical Approach. *Biophysical Journal* **72**, 595-612, (1997).

58. Fang, F. & Szleifer, I. Controlled release of proteins from polymer-modified surfaces. *Proc Natl Acad Sci U S A* **103**, 5769-5774, (2006).

59. Todeschini, R. & Consonni, V. in *Handbook of Chemoinformatics: From Data to Knowledge in 4 Volumes* (ed J. Gasteiger) Ch. VIII.2, 1004-1033 (WILEY−VCH Verlag GmbH & Co. KgaA, 2003).

60. Yu, Y. *et al.* Multifunctional "Hydrogel Skins" on Diverse Polymers with Arbitrary Shapes. *Adv Mater* **31**, e1807101, (2019).

61. Lee, K. Y. *et al.* Controlling Mechanical and Swelling Properties of Alginate Hydrogels Independently by Cross-Linker Type and Cross-Linking Density. *Macromolecules* **33**, 4291-4294, (2000).

62. Jeong, J. W. *et al.* Soft materials in neuroengineering for hard problems in neuroscience. *Neuron* **86**, 175-186, (2015).

63. Lacour, S. P., Courtine, G. & Guck, J. Materials and technologies for soft implantable neuroprostheses. *Nature Reviews Materials* **1**, (2016).

64. Onuki, Y., Bhardwaj, U., Papadimitrakopoulos, F. & Burgess, D. J. A Review of the Biocompatibility of Implantable Devices: Current Challenges to Overcome Foreign Body Response. *Journal of Diabetes Science and Technology* **2**, 1003-1015, (2008).

65. Teo, A. J. T. *et al.* Polymeric Biomaterials for Medical Implants and Devices. *ACS Biomaterials Science & Engineering* **2**, 454-472, (2016).

66. Kozai, T. D. *et al.* Mechanical failure modes of chronically implanted planar silicon-based neural probes for laminar recording. *Biomaterials* **37**, 25-39, (2015).

67. Barfidokht, A. & Gooding, J. J. Approaches Toward Allowing Electroanalytical Devices to be Used in Biological Fluids. *Electroanalysis* **26**, 1182-1196, (2014).

68. Labib, M., Sargent, E. H. & Kelley, S. O. Electrochemical Methods for the Analysis of Clinically Relevant Biomolecules. *Chem Rev* **116**, 9001-9090, (2016).

69. Maji, D. *et al.* ClotChip: A Microfluidic Dielectric Sensor for Point-of-Care Assessment of Hemostasis. *IEEE Trans. Biomed. Circuits Syst.* **11**, 1459-1469, (2017).

70. Toyoda, T. *et al.* Direct activation of platelets by addition of CaCl2 leads coagulation of platelet-rich plasma. *Int J Implant Dent* **4**, 23, (2018).

71. Elgrishi, N. *et al.* A Practical Beginner's Guide to Cyclic Voltammetry. *Journal of Chemical Education* **95**, 197-206, (2017).

72. Sandford, C. *et al.* A synthetic chemist's guide to electroanalytical tools for studying reaction mechanisms. *Chem Sci* **10**, 6404-6422, (2019).

73. Ellington, A. D. In vitro selection of RNA molecules that bind specific ligands. *Nature* **346**, 818-822, (1990).

74. Bock, L. C., Griffin, L. C., Latham, J. A., Vermaas, E. H. & Toole, J. J. Selection of single-stranded DNA molecules that bind and inhibit human thrombin. *Nature* **355**, 564-566, (1992).

75. Song, S., Wang, L., Li, J., Fan, C. & Zhao, J. Aptamer-based biosensors. *TrAC Trends in Analytical Chemistry* **27**, 108-117, (2008).

76. Gold, L. SELEX: How It Happened and Where It will Go. *J Mol Evol* **81**, 140-143, (2015).

77. Ferguson, B. S. *et al.* Real-Time, Aptamer-Based Tracking of Circulating Therapeutic Agents in Living Animals. *Science Translational Medicine* **5**, 1-9, (2013).

78. Arroyo-Currás, N. *et al.* High-Precision Control of Plasma Drug Levels Using Feedback-Controlled Dosing. *ACS Pharmacology & Translational Science* **1**, 110-118, (2018).

79. Mage, P. L. *et al.* Closed-loop control of circulating drug levels in live animals. *Nature Biomedical Engineering* **1**, (2017).

80. Arroyo-Currás, N., Dauphin-Ducharme, P., Scida, K. & Chávez, J. L. From the beaker to the body: translational challenges for electrochemical, aptamer-based sensors. *Analytical Methods* **12**, 1288-1310, (2020).

81. Lovering, A. M. & Reeves, D. S. in *Antibiotic and Chemotherapy* Ch. 12, 145-169 (Elsevier, 2011).

82. Artuğ, G., Roosmasari, I., Richau, K. & Hapke, J. A Comprehensive Characterization of Commercial Nanofiltration Membranes. *Separation Science and Technology* **42**, 2947-2986, (2007).

83. Van der Bruggen, B. Chemical modification of polyethersulfone nanofiltration membranes: A review. *Journal of Applied Polymer Science* **114**, 630-642, (2009).

84. Yoshida, W. *et al.* Selection of DNA aptamers against insulin and construction of an aptameric enzyme subunit for insulin sensing. *Biosens Bioelectron* **24**, 1116-1120, (2009).

85. Dahe, G. J. *et al.* In vivo evaluation of the biocompatibility of surface modified hemodialysis polysulfone hollow fibers in rat. *PLoS One* **6**, e25236, (2011).

86. Arroyo-Curras, N. *et al.* Real-time measurement of small molecules directly in awake, ambulatory animals. *Proc Natl Acad Sci U S A* **114**, 645-650, (2017).

87. Romero-Reyes, M. A. & Heemstra, J. M. Small-Molecule Sequestration Using Aptamer-Functionalized Membranes. *ACS Materials Letters* **1**, 568-572, (2019).

88. Yu, H., Xu, Z., Lei, H., Hu, M. & Yang, Q. Photoinduced graft polymerization of acrylamide on polypropylene microporous membranes for the improvement of antifouling characteristics in a submerged membrane-bioreactor. *Separation and Purification Technology* **53**, 119-125, (2007).

89. Zhao, C. *et al.* Antifouling and biodegradable poly(N-hydroxyethyl acrylamide) (polyHEAA)-based nanogels. *RSC Advances* **3**, (2013).

90. Mondal, S. & Wickramasinghe, S. R. Photo-induced graft polymerization of N-isopropyl acrylamide on thin film composite membrane: Produced water treatment and antifouling properties. *Separation and Purification Technology* **90**, 231-238, (2012).

91. Caulfield, M. J., Qiao, G. G. & Solomon, D. H. Some Aspects of the Properties and Degradation of Polyacrylamides. *Chemical Reviews* **102**, 3067-3084, (2002).

92. Nishiyama, N. Hydrolytic stability of methacrylamide in acidic aqueous solution. *Biomaterials* **25**, 965-969, (2004).

93. Norde, W. & Haynes, C. A. (ed Horbett and Brash) Ch. 2, 26-40 (American Chemical society, 1995).

94. Campuzano, S., Pedrero, M., Yanez-Sedeno, P. & Pingarron, J. M. Antifouling (Bio)materials for Electrochemical (Bio)sensing. *Int J Mol Sci* **20**, (2019).

95. Xiong, R. *et al.* Sizing nanomaterials in bio-fluids by cFRAP enables protein aggregation measurements and diagnosis of bio-barrier permeability. *Nat Commun* **7**, 12982, (2016).

96. Tong, J. & Anderson, J. L. Partitioning and Diffusion of Proteins and Linear Polymers in Polyacrylamide Gels. *Biophysical Journal* **70**, 1505-1513, (1996).

97. Hagel, V., Haraszti, T. & Boehm, H. Diffusion and Interaction in PEG-DA hydrogels. *Biointerfaces* **8**, 1-9, (2013).

Supplementary Information

Combinatorial Polyacrylamide Hydrogels for Preventing Biofouling on Implantable Biosensors

Doreen Chan[1,2,], Jun-Chau Chien[3,*], Eneko Axpe[2], Louis Blankemeier[3], Samuel W. Baker[4], Sarath Swaminathan[5], Victoria A. Piunova[5], Dmitry Yu. Zubarev[5], H. Tom Soh[6,7,8,†], Eric A. Appel[2,8,9,10,†]*

[1]Department of Chemistry, Stanford University, Stanford, CA 94305, USA.

[2]Department of Materials Science & Engineering, Stanford University, Stanford, CA 94305, USA.

[3]Department of Electrical Engineering, Stanford University, Stanford, CA 94305, USA.

[4]Deparment of Comparative Medicine, Stanford University, Stanford, CA 94305, USA.

[5]IBM Almaden Research Center San Jose, CA 95120, USA.

[6]Department of Radiology, Stanford University, Stanford, CA 94305, USA.

[7]Chan Zuckerberg Biohub, San Francisco, CA 94158, USA.

[8]ChEM-H Institute, Stanford University, Stanford, CA 94305, USA.

[9]Department of Bioengineering, Stanford University, Stanford, CA 94305, USA.

[10]Department of Pediatrics (Endocrinology), Stanford University, Stanford, CA 94305, USA.

**These authors contributed equally.*

[†]Correspondence to: eappel@stanford.edu, tsoh@stanford.edu

Table of Contents

Figure S1. Platelet adhesion screening with combinatorial polyacrylamide hydrogels. 3

Figure S2. Contribution of monomers and features in biofouling performance. 4

Table S1. Performance of random forest classifier on the withheld test set with different features generated for the polymers. 5

Table S2. Definitions of molecular descriptors. 6

Figure S3. Complete list of feature importance for each monomer from Feature Set B. 8

Figure S4. Heterogeneity of the platelet coverage suggests steric mode of fouling. 10

Figure S5. Mechanical and physical properties of F50-C50 hydrogel 11

Figure S6. Addition of calcium chloride expedites blood occlusion completely after 6 hr. 12

Figure S7. Raw data for in vitro electrochemical device fouling assay (after 2 hr with $CaCl_2$ addition). 12

Figure S8. Raw data for in vivo electrochemical device fouling assay after 5 days. 13

Figure S9. SEM Micrographs of aptamer probes. 13

Figure S11. DNA aptamer probes after flowing whole blood assay. 15

Figure S12. Raw data for real-time in vivo sensing of kanamycin with ~95 minute stabilization period. 16

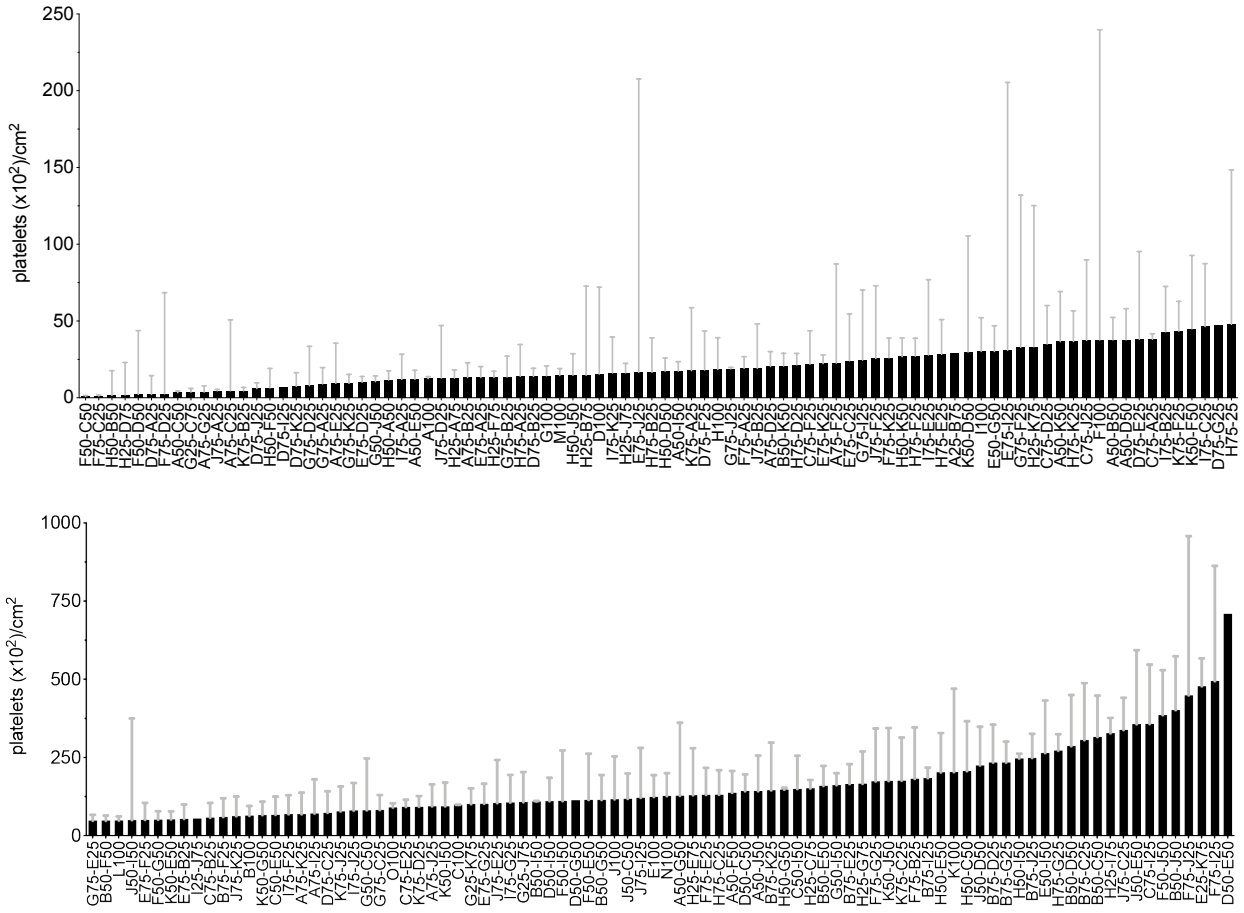

Figure S1. Platelet adhesion screening with combinatorial polyacrylamide hydrogels. Median ± SD platelet counts on hydrogel surfaces are shown with n ≥ 3.

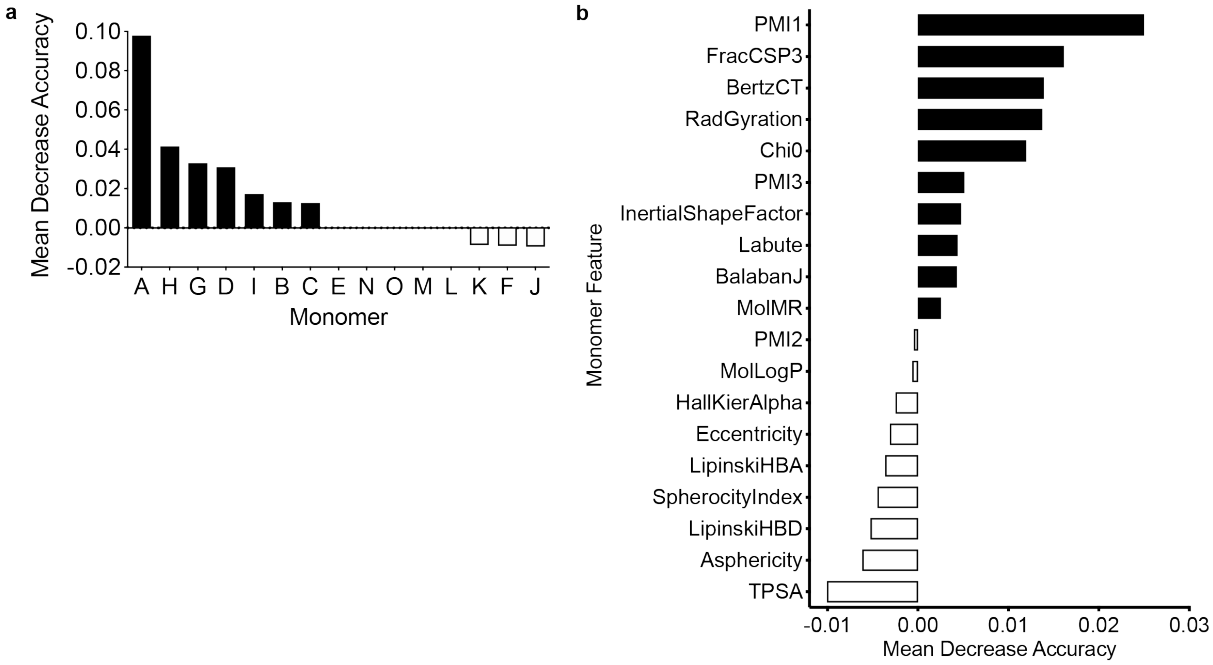

Figure S2. Contribution of monomers and features in biofouling performance. a. MDA feature relevance evaluated with feature set A that accounts for the monomer type and includes molar ratios as scaling factors. Monomers A, H, and G exhibited highest MDA, indicating high extent to which the feature is important for model development. **b.** Feature importance with Feature Set C. Positive MDA values indicate high relevance.

Table S1. Performance of random forest classifier on the withheld test set with different features generated for the polymers.

Feature Set A

	precision	**recall**	**f1-score**	**support**
0	0.71	0.79	0.75	19
1	0.81	0.74	0.77	23
micro avg	0.76	0.76	0.76	42
macro avg	0.76	0.76	0.76	42
weighted avg	0.77	0.76	0.76	42

Feature Set B

	precision	**recall**	**f1-score**	**support**
0	0.71	0.79	0.75	19
1	0.81	0.74	0.77	23
micro avg	0.76	0.76	0.76	42
macro avg	0.76	0.76	0.76	42
weighted avg	0.77	0.76	0.76	42

Feature Set C

	precision	**recall**	**f1-score**	**support**
0	0.65	0.79	0.71	19
1	0.79	0.65	0.71	23
micro avg	0.71	0.71	0.71	42
macro avg	0.72	0.72	0.71	42
weighted avg	0.73	0.71	0.71	42

Table S2. Definitions of molecular descriptors.

Physical-Chemical Descriptors		**References**
LabuteASA	*approximate surface area per Labute definition*	*J. Mol. Graph. Mod.* **18**:464-77 (2000).
TPSA	*topological polar surface area*	*J. Med. Chem.* **43**:3714-7, (2000) .
MolLogP	*partition coefficient, measure of lipophilicty*	Wildman and Crippen *JCICS* **39**:868-73 (1999).
MolMR	*molar refractivity*	Wildman and Crippen *JCICS* **39**:868-73 (1999).
Molecular Graph Descriptors		
BalabanJ	*averaged distance sum connectivity, related to number of bonds between two vertices*	*Chem. Phys. Lett.* **89**:399-404 (1982).
BertzCT	*index of molecular complexity due to distribution of the heteroatoms and complexity of the bonding*	*J. Am. Chem. Soc.* **103**:3599-601 (1981).
Chi0	*valence connectivity index*	*Rev. Comput. Chem.* **2**:367-422 (1991).
HallKierAlpha	*describes number of atoms and number of connectivities*	*Rev. Comput. Chem.* **2**:367-422 (1991).
H-bonding Descriptors		
LipinskiHBA	*number of Ns and Os in the molecule*	-
LipinskiHBD	*number of N-H and O-H bonds in a molecule*	-
3D Shape Descriptors		
FracCSP3	*number of tetrahedral carbon atoms*	-
InertialShapeFactor	*shape measured based on principle moments of inertia*	G. A. Arteca “Molecular Shape Descriptors” Reviews in Computational Chemistry vol 9.
PMI1	*first (smallest) principle moment of inertia*	-
PMI2	*second principle moment of inertia*	-
PMI3	*third (largest) principle moment of inertia*	-
RadGyration	*radius of gyration*	G. A. Arteca “Molecular Shape Descriptors” Reviews in Computational Chemistry vol 9.
SpherocityIndex	*index of resemblance to that of a perfect sphere*	Todeschini and Consoni “Descriptors from Molecular Geometry” Handbook of Chemoinformatics.
Asphericity	*measurement of the shape of a refractive molecule and its effect on the bending of light*	A. Baumgaertner, “Shapes of flexible vesicles” J. Chem. Phys. 98:7496 (1993).

Eccentricity	*measurement of the maximum distances from one atom vertex to any other atom vertex*	G. A. Arteca “Molecular Shape Descriptors” Reviews in Computational Chemistry vol 9.

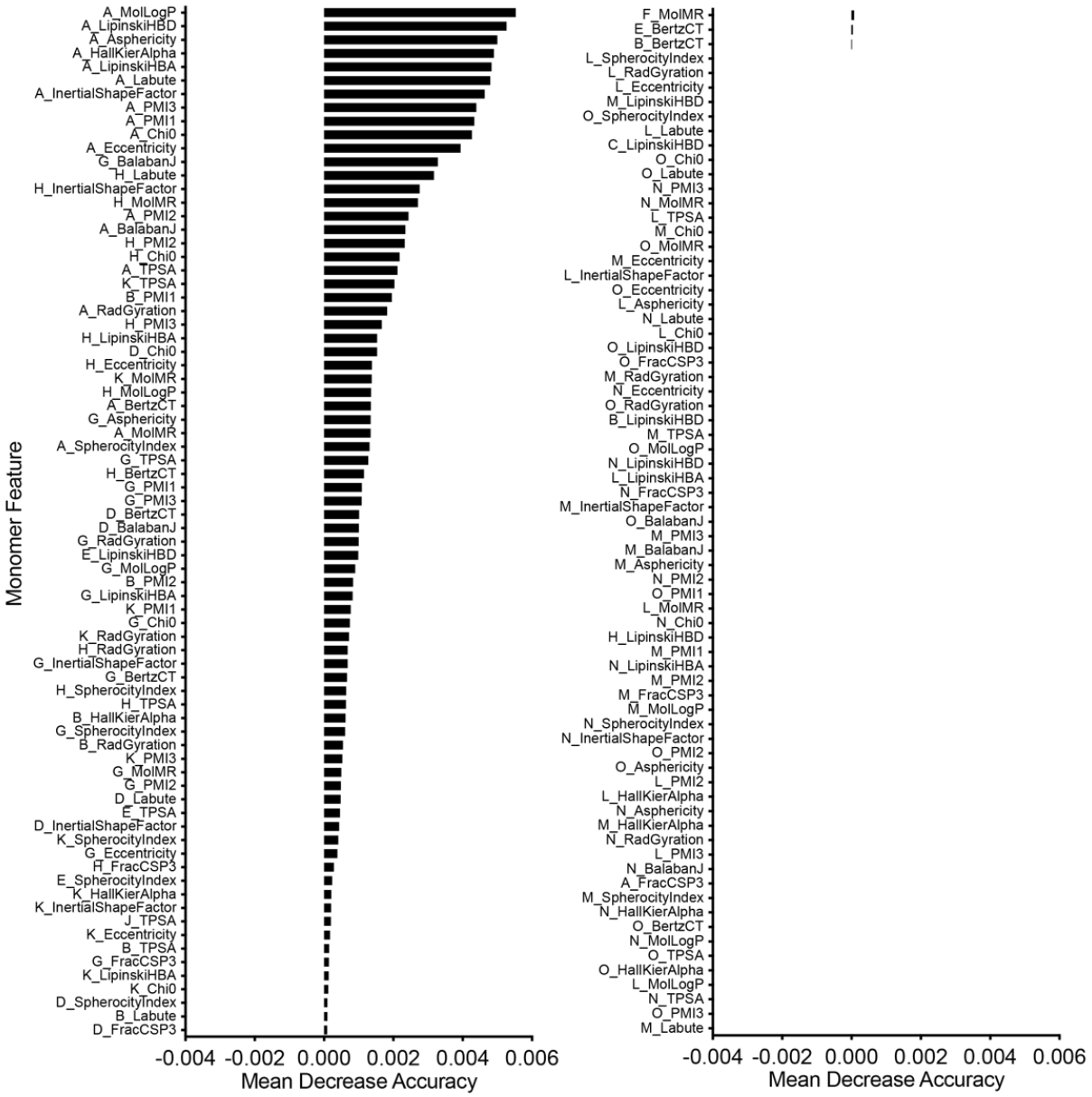

Figure S3. Complete list of feature importance for each monomer from Feature Set B. Positive MDA values indicate high impact of the feature (monomer-specific descriptor) to the model performance while negative MDA values indicate irrelevance of the feature.

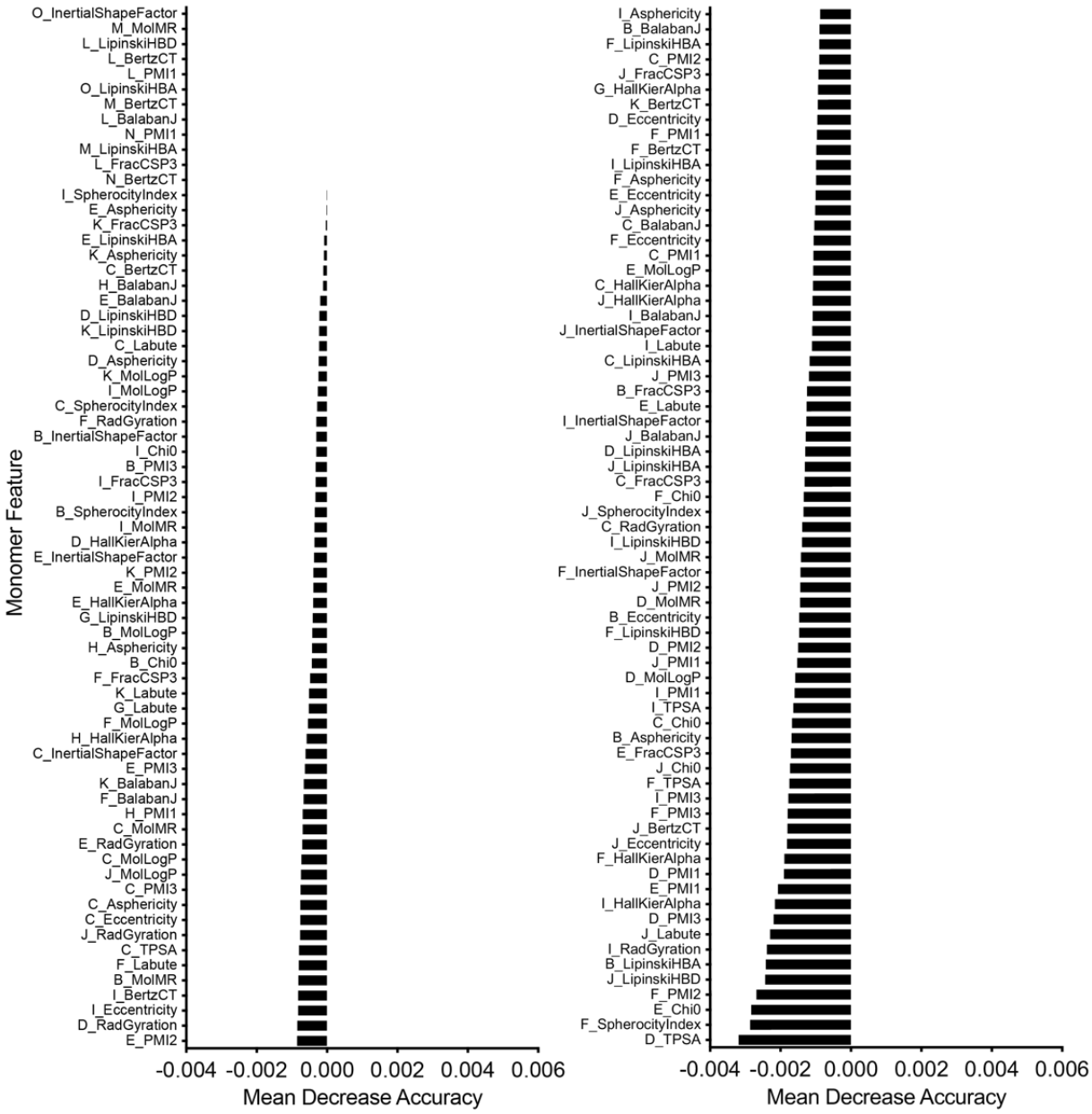

Figure S3 (*continued*). Complete list of feature importance for each monomer from Feature Set B. Positive MDA values indicate high impact of the feature (monomer-specific descriptor) to the model performance while negative MDA values indicate irrelevance of the feature.

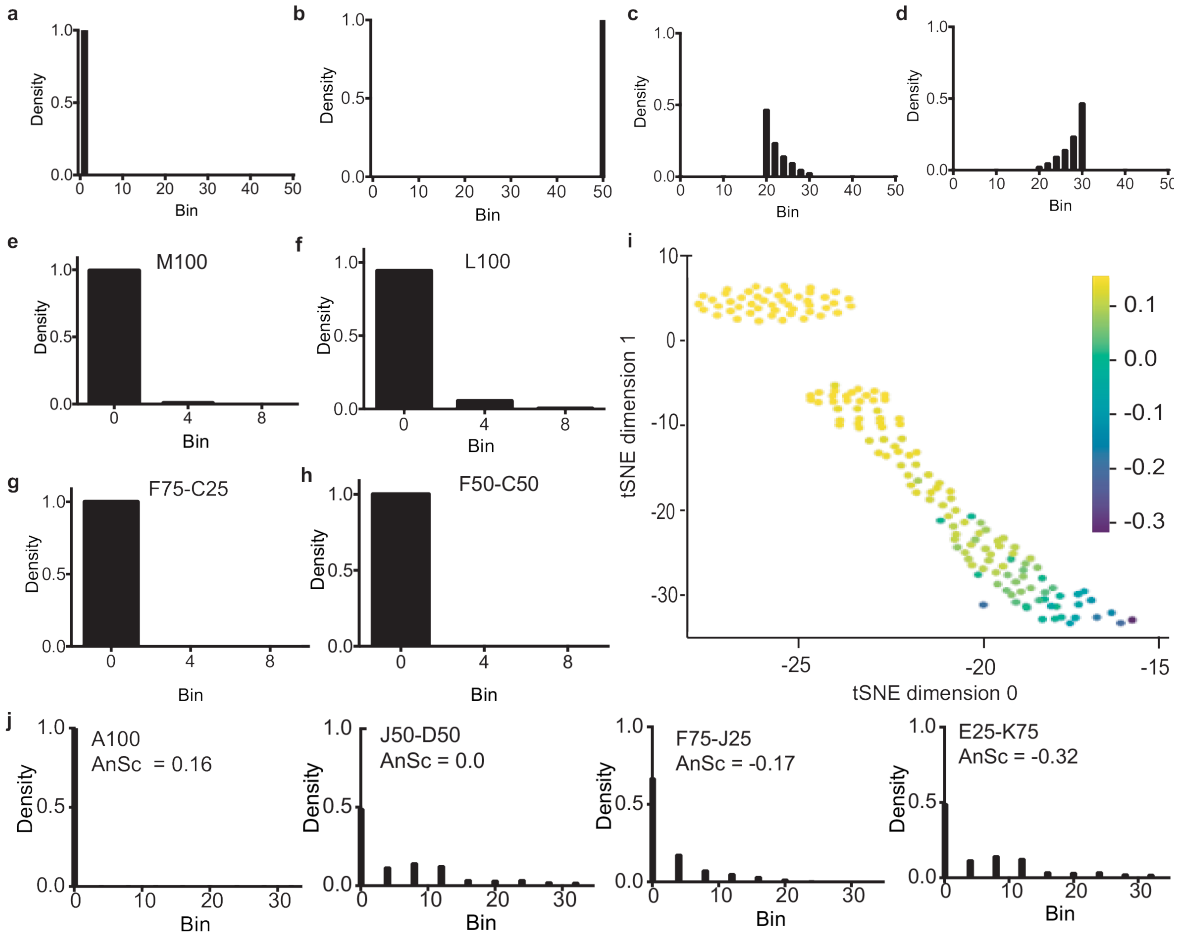

Figure S4. Heterogeneity of the platelet coverage suggests steric mode of fouling. General types of population histograms that might be encountered: **a.** homogenous coverage, empty surface; **b**. homogenous coverage, uniformly covered surface; **c.** heterogenous coverage, covered surface with dense coverage domains. **d.** heterogenous coverage, covered surface with sparse domains. **e.** Population histogram of M100. **f.** Population histogram of L100. **g.** Population histogram of F75-C25. **h.** Population histogram of F50-C50. **i.** Results of the outlier detection in the manifold embedding of the population histograms via t-SNE algorithm. Color encodes the anomaly score of the sample obtained via Isolation Forest algorithm. Negative values of the anomaly score indicate outliers; high positive values indicate normal samples. **j.** Examples of population histograms, from the highest value (the group of the most normal samples, outlined by the box), to the lowest anomaly score (the most abnormal sample).

a

Physical/Mechanical Property	Technique	Value (Mean ± S.D.)
G'	Rheology	29.8 ± 3.0 kPa
G"	Rheology	4.8 ± 1.2 kPa
E	Nanoindentation	1.0 ± 0.1 MPa
E	Tensile Test	1.9 ± 0.2 kPa
Toughness	Tensile Test	0.92 ± 0.42 J/m^3
Strain at Break	Tensile Test	35.1 ± 6.0 %
Mesh Size	FRAP	2.3 ± 0.1 nm

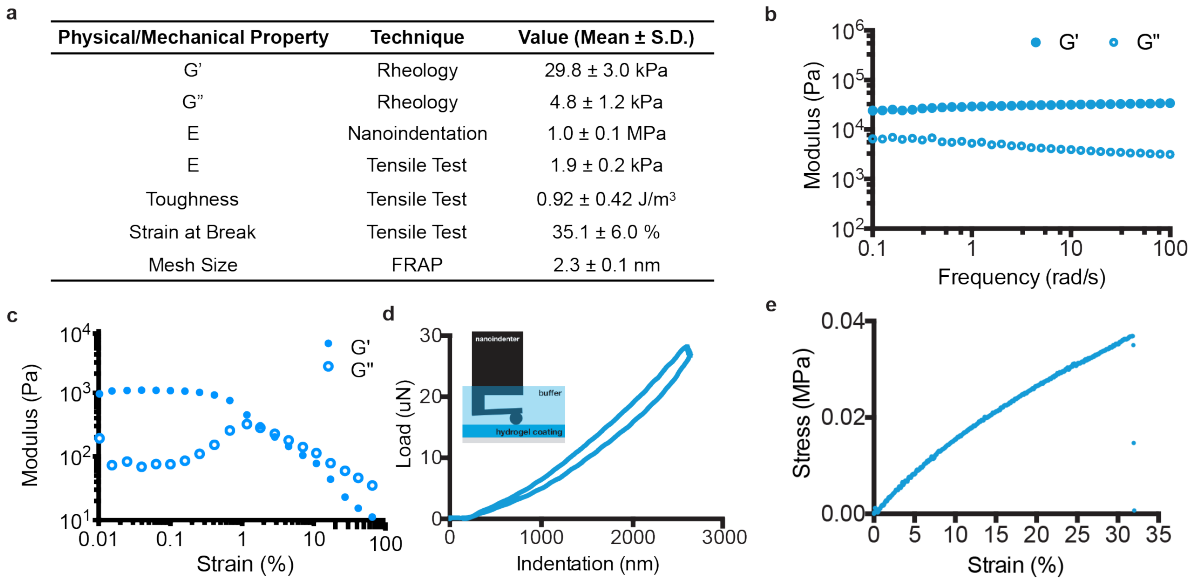

Figure S5. Mechanical and physical properties of F50-C50 hydrogel. a. Summary of measured mechanical properties. **b.** Frequency-dependent rheological properties (1% strain) of polyacrylamide hydrogels with low and high molecular weight monomers demonstrates that the resulting hydrogels exhibit only minor variations in observed *G'* and *G"* values. **c.** Amplitude-dependent rheological properties for the F50-C50 hydrogel at 10 rad/s. **d.** Representative curve of nanoindentation loading and unloading. **e.** Representative tensile test of F50-C50 hydrogel.

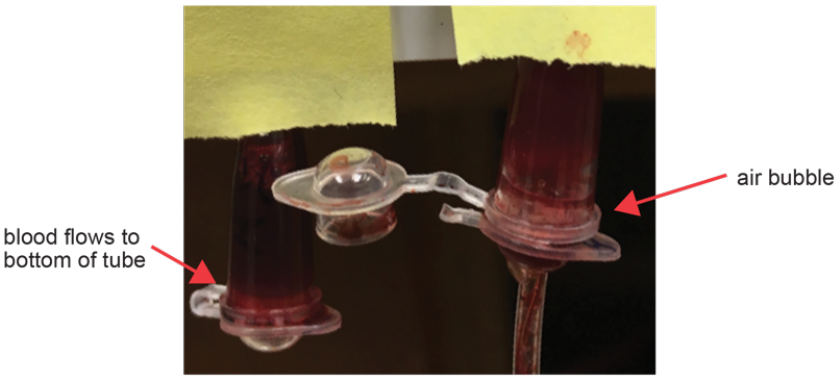

Figure S6. Addition of calcium chloride expedites blood occlusion completely after 6 hr. With no $CaCl_2$ addition (left), blood flows. With $CaCl_2$ addition, blood clots and does not fall in the tube upon inversion (right).

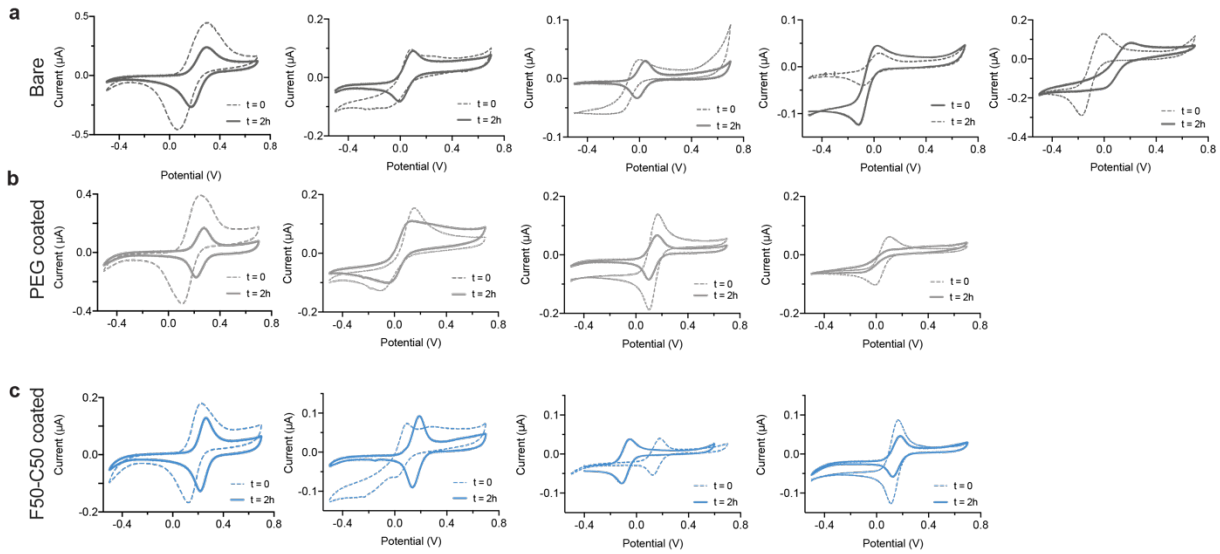

Figure S7. Raw data for in vitro electrochemical device fouling assay (after 2 hr with $CaCl_2$ addition). a. Bare probe shows significant signal degradation. **b.** PEG coated device. **c.** F50-C50 coated device.

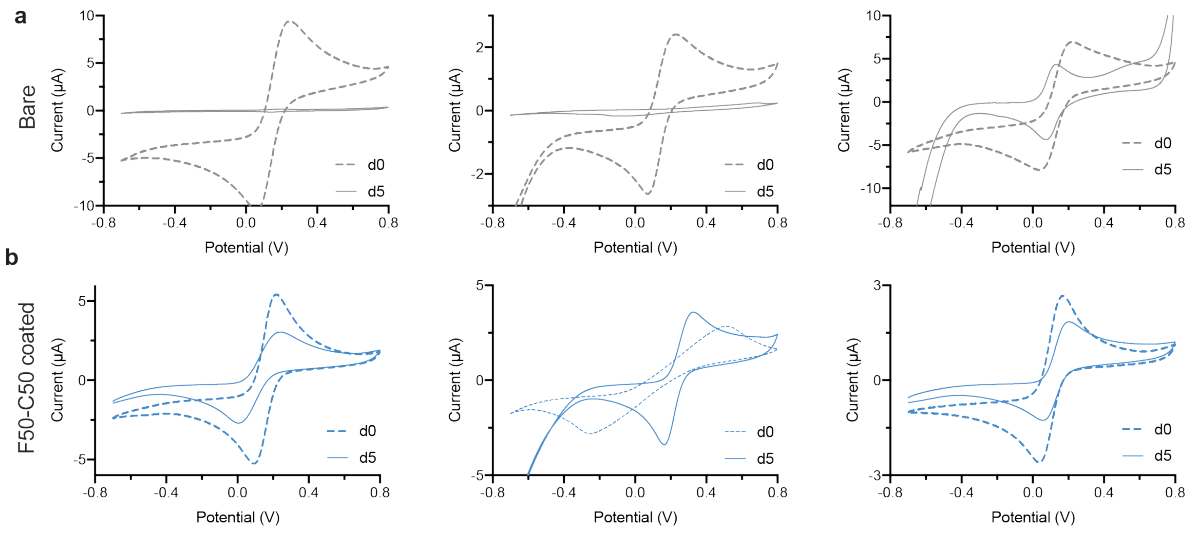

Figure S8. Raw data for in vivo electrochemical device fouling assay after 5 days. a. Bare probe shows significant signal degradation. **b.** F50-C50 coated device.

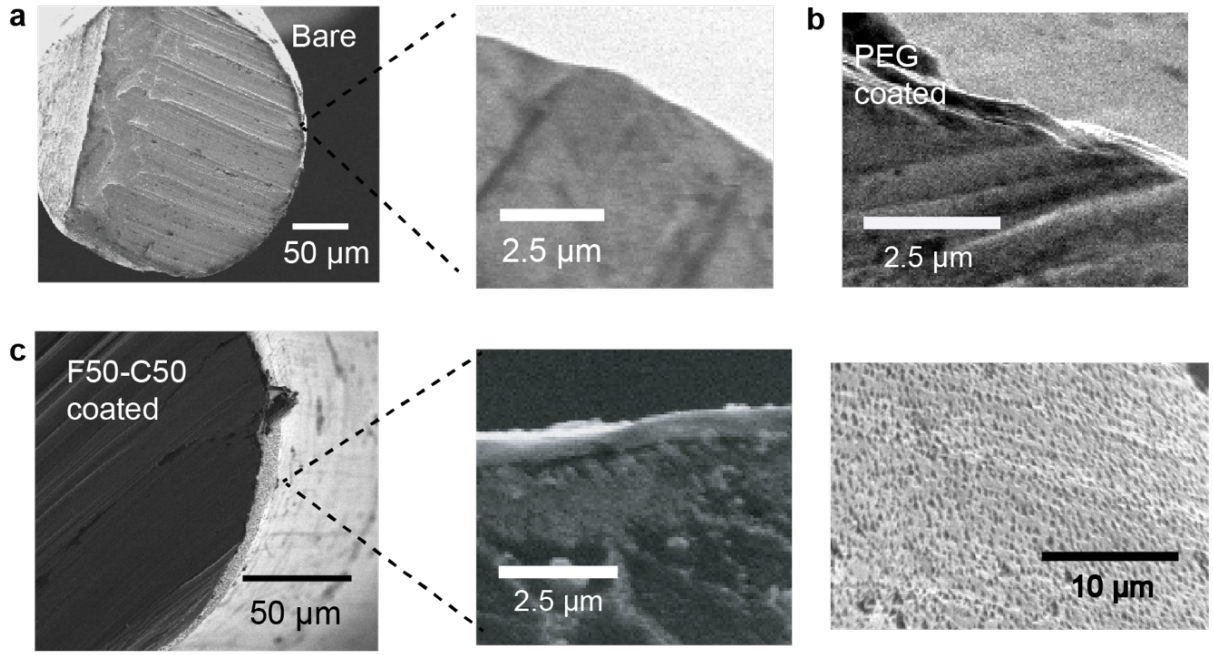

Figure S9. SEM Micrographs of aptamer probes. a. Bare aptamer sensor. **b.** PEG-coated aptamer sensor. **c.** F50-C50 coated aptamer sensor.

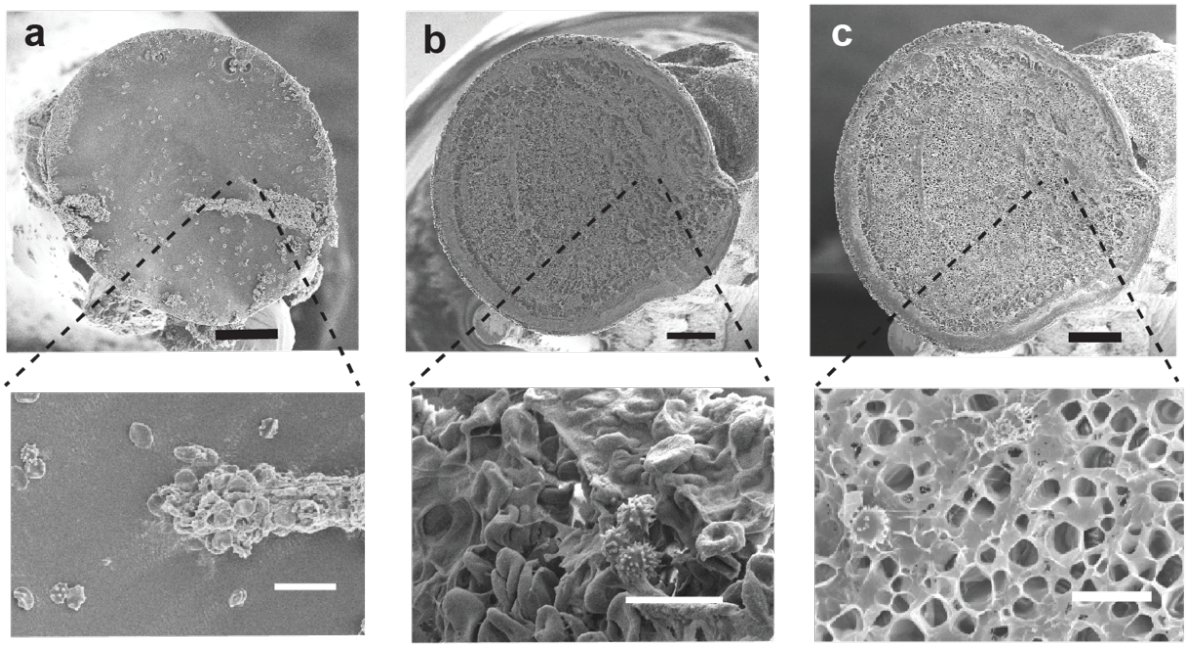

Figure S10. DNA aptamer probes after incubation in whole blood assay after 3 days. a. Platelet adhesion and activation on the tip of the bare probe. **b.** PEG-coated hydrogel shows coverage from platelet agglomeration. **c.** Homogenous coating of F50-C50 gel remains visible with less adhesion of platelets. White bar = 10 μm. Black bar = 100 μm.

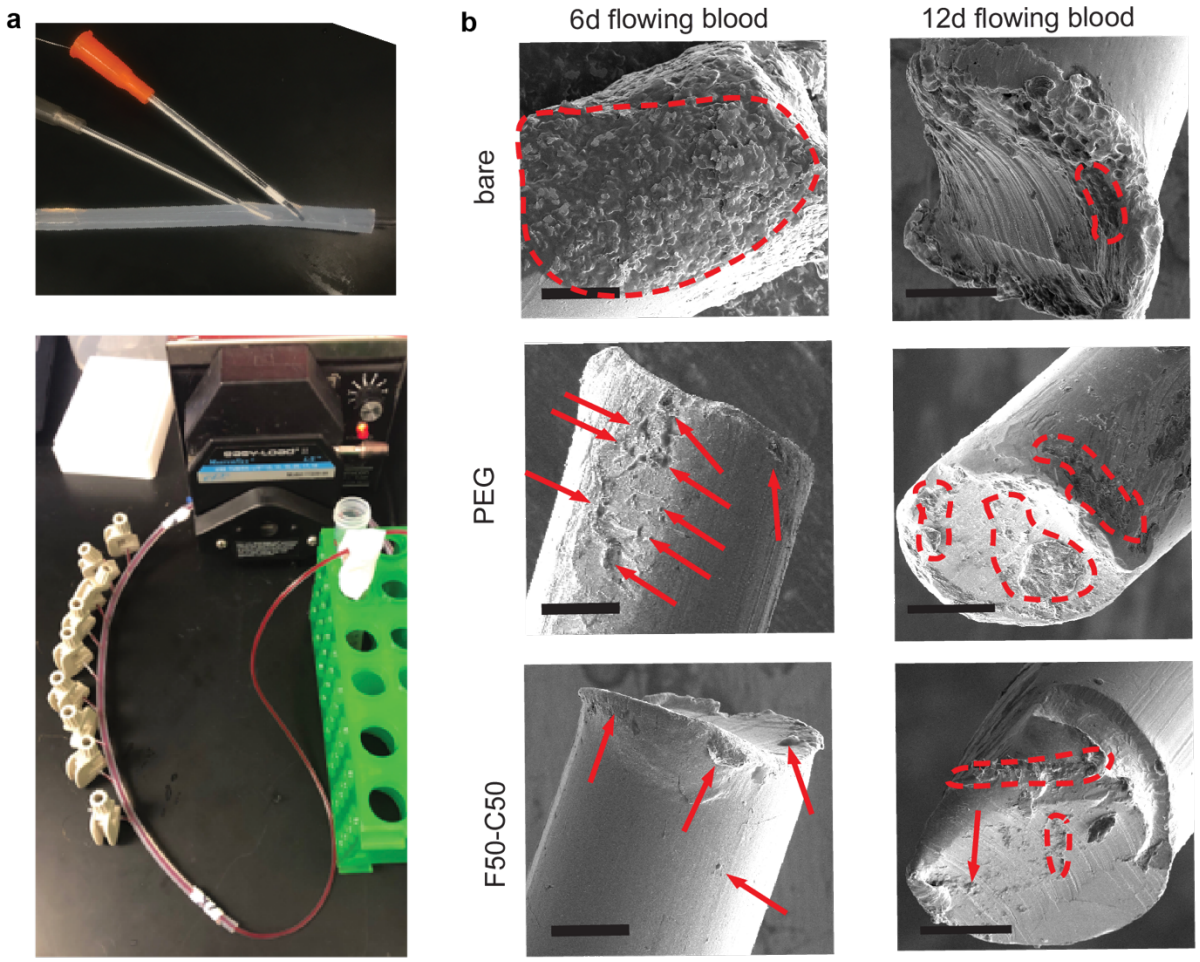

Figure S11. DNA aptamer probes after flowing whole blood assay. a. *in vitro* whole blood flowing assay. Probes are inserted through a catheter into a closed loop blood pumping system. **b.** SEM Micrographs of the hydrogel coating on DNA aptamer probes, and the probe tips after 6 days and 12 days in flowing blood. Scale bar = 30 μm.

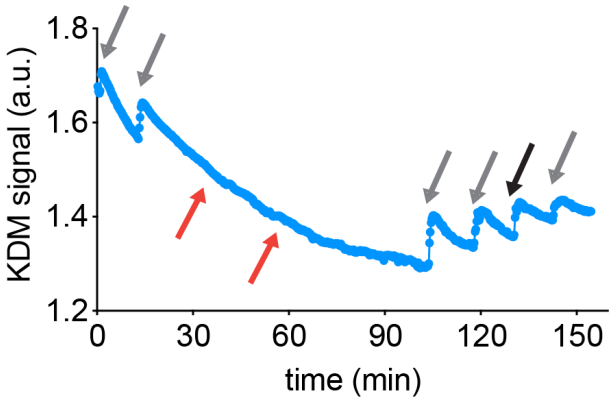

Figure S12. Raw data for real-time in vivo sensing of kanamycin with ~95 minute stabilization period. Gray arrows represent a 100 μL injection of 100 mM kanamycin and the solid black arrow represents a 200 μL injection of 100 mM kanamycin. Red arrows represent injection of 500 μL of 25 mM ampicillin. The absence of peaks associated with ampicillin administration indicates aptamer specificity is preserved for kanamycin.